People's Democratic Republic of Algeria
Ministry of Higher Education and Scientific Research

Echahid Hamma Lakhdar University of El-Oued
FACULTY OF TECHNOLOGY

End of study dissertation

Presented for graduation from

MASTER ACADEMIQUE

Domain:Science and Technology

Department: Mechanical Engineering

Specialty: Energetic mechanics

Theme

Comparative study between CFD and BEM theory to optimize the wind turbine performance

Submitted by:

- BACI Mohammed Maamar
- BACI Ahmed Mohammed
- DOUDI Abdelhamid
- MENNAI Yacine

The jury composed of :

President	Dr,Mezian Asia	**MAA**	El-Oued University
Examiner	Dr,Ali Zine	**MAA**	El-Oued University
Examiner	Dr,Atia Abdelmalek	**Dr**	El-Oued University
Supervisor	Dr,Gherbi Med Tahar	**MAA**	El-Oued University

2021-2022

THANKS

We would like to thank ALLAH who gave us the courage and the will to carry out this modest work.

All our gratitude for our supervisor Mr. GHERBI Mohammed Tahar, and Mr. DEGHOUM Khalil for his very precious help, his disposition, his kindness, and his advice.

We would like to express our sincere thanks to all the personnel of the mechanical engineering department and to all the people who have contributed directly or indirectly to the realization and success of this work.

Abstract

Wind energy is an important resource in the field of renewable energies. In this study, two different methods were adopted to study wind turbines and compare them to determine the simplest and most accurate. Using the theory of blade element momentum (BEM) and computational fluid dynamics (CFD), the blade of a wind turbine with a power of 10 kW was analyzed to calculate the power coefficient and torque coefficient as well as calculate the power. According to the obtained results, it was found that the BEM theory is simpler and easier to use by relying on a 2D blade element. In contrast, CFD relies on 3D simulations and this is what makes it more accurate in describing the studied model.

Key words: Q Blade, Computational Fluid Dynamics (CFD), Horizontal wind turbine, Blade Element Momentum (BEM), Wind Energy.

ملخص

تعد طاقة الرياح موردًا مهمًا في مجال الطاقات المتجددة. في هذه الدراسة تم اعتماد طريقتين مختلفتين لدراسة توربينات الرياح ومقارنتها لتحديد الأبسط والأكثر دقة. باستخدام نظرية زخم عنصر الشفرة (BEM) وديناميكيات السوائل الحسابية (CFD) ، تم تحليل شفرة توربين الرياح بقوة 10 كيلو وات لحساب معامل القدرة ومعامل عزم الدوران وكذلك حساب القدرة. وفقًا للنتائج التي تم الحصول عليها ، وجد أن نظرية BEM أبسط وأسهل في الاستخدام من خلال الاعتماد على عنصر شفرة ثنائية الأبعاد. في المقابل ، يعتمد CFD على المحاكاة ثلاثية الأبعاد وهذا ما يجعله أكثر دقة في وصف النموذج المدروس.

الكلمات المفتاحية :

QBLADE, ديناميكيات السوائل الحسابية (CFD), تربينات الرياح الافقية, زخم عنصر الشفرة (BEM), طاقة الرياح.

Résumé

L'énergie éolienne est une ressource importante dans le domaine des énergies renouvelables. Dans cette étude, deux méthodes différentes ont été adoptées pour étudier les éoliennes et les comparer pour déterminer la plus simple et la plus précise. En utilisant la théorie de la quantité de mouvement des éléments de pale (BEM) et la dynamique des fluides computationnelle (CFD), la pale d'une éolienne d'une puissance de 10 kW a été analysée pour calculer le coefficient de puissance et le coefficient de couple ainsi que pour calculer la puissance. Selon les résultats obtenus, il a été constaté que la théorie BEM est plus simple et plus facile à utiliser en s'appuyant sur un élément de lame 2D. En revanche, la CFD s'appuie sur des simulations 3D et c'est ce qui la rend plus précise dans la description du modèle étudié.

Mots-clés : QBlade, dynamique des fluides de calcul (CFD), éolienne horizontale, élan de l'élément lame (BEM), énergie éolienne.

Index

List of table

Listed of figures

Table of Nomenclature :

C_p	specific heat capacity of the air, j kg-1 k-1
ρ	density, kg m-3
A	moment coefficient
V^3	cubic volume
T	temperature
Δp	the pressure drops over the rotor
c	chord length
$\emptyset$	inflow angle
U	speed of rotor at the tip of blades
V	wind speed
R	blade radius
ω	rotational velocity in (radians/second)
C_L	lift ratio
A	area of the rotor
λ	tip-speed ratio
C_m	moment coefficient
W^2	relative wind
C_D	drag lift
C_T	tangential force
C_N	normal force
B	number of baldes
r	disk radius
β	twist angle of the blade
θ	pitch angle of the blade
θ	combination of the twist angle
θp	pitch of angle
V	undisturbed wind velocity
Δa	maximum value
$\Delta a'$	below the convergence criterion
$\emptyset$	flow angle
V_a	equivalent angle of attack
a'	tangential induction factor
λ_r	the local tip speed ratio
c	chord length of the blade section
C_l	lift coefficient at the angle of the attack
In	Inlet
Out	Outlet
%	percentage
m	Meter
s	Second

Introduction

GENERAL INTRODUCTION:

The importance of renewable energy sources gradually increases with climate change. One of the renewable energy sources is wind. Nowadays, the number of green energy systems is increasing day by day and also, small size wind turbines are designed for the purpose of using in greenhouses.

Energy sources based on fossil fuels increase carbon dioxide emissions, therefore, studies on alternative energy sources and wind are one of the most important sources. That's why we need wind turbines to harness wind energy.

Two types of wind turbines are commonly used. One is horizontal wind turbine and the other is vertical wind turbine and in the first chapter we will explain more about wind turbine types, components, airfoils, materials and pros and cons.

A wind turbine converts wind energy into electricity by using the aerodynamic force from the rotor blades, which act like the wing of an airplane or the rotor blades of a helicopter. When air blows over the blade, the air pressure on one side of the blade is reduced. The difference in air pressure on both sides of the blade creates both lift and drag. The force of lift is stronger than the drag and this causes the rotor to spin. The rotor connects to the generator, either directly (if it is a direct drive turbine) or by means of a shaft and a series of gears (a gearbox) that speed up rotation and allow a physically smaller generator. This translation of the aerodynamic force to the generator's rotation creates electricity. Therefore, we choose to talk about wind turbine aerodynamics in the second chapter.

The third chapter explains more about how to predict the aerodynamic performance of wind turbines, in our study, we select a 10kw horizontal wind turbine with a rotor diameter of 6 m and S809 as an airfoil, Q Blade and Aerodynamic performance is predicted using Ansys-. fluent. First, the turbine is designed and achieved aerodynamic performance by the software QBlade under a general public license. After that, the domain construction and grid construction are described to calculate the 3D wind turbine performance. Then, the aerodynamic performance is calculated using CFD methods (Fluent Commercial Software). Finally, the turbine power and torque coefficient curves obtained by the 3D CFD results are compared with the QBlade results.

Chapitre I

Generality about Wind Turbines

I.1.INTRODUCTION:

Wind turbines are machines that take kinetic energy from the wind and transform it into mechanical energy, which is then translated into a more usable form of electricity.

Wind energy is currently responsible for around 10% of the world's energy supply, and its role in the renewable energy industry is only expected to rise as its potential is recognized. Optimization of wind turbine efficiency is crucial to remaining competitive with existing technologies, and it is complemented by a wise choice of horizontal or vertical orientation and materials as decided by engineering design. Furthermore, the material should be long-lasting, ideally recyclable, and low-cost to produce so that the favorable environmental impact and economic benefits of wind power are not negated.

We choose to discuss wind turbines, types, airfoils, materials, and pros and disadvantages in this chapter to further clarify our memoir.

I.2.BIBLIOGRAPHIC SEARCH:

J. Aramach and all[1],_In this work, an advanced approach to the aerodynamic simulation of a wind turbine rotor is introduced. Two numerical codes (AEROC and EOLI), developed by the authors and based on a robust viscous–inviscid interaction technique and modified BEM theory, respectively, were used in the final step to characterize the rotor blade airfoil and evaluate its performance, The developed codes were validated by comparison with experimental data and mathematical models found in the scientific literature.

Sandeep. A and all [2], Multiple iterations of blades with a length of 800 mm have been successfully constructed for horizontal axis micro wind turbines with a power output of 600 watts. The chord of the optimized blade is decreased by 24%, while the thickness is lowered by 44%. When compared to a standard blade, the power coefficient of the optimized blade is improved by up to 30%.

Sanjay Singh Bhadauria and of all [3], The blades of a wind turbine are the most expensive part. A wind turbine's power output is ideally proportional to the square of the blade length. Due to the high material cost and size, the blade's construction and operation necessitate extreme caution. Glass-epoxy composites are a common composite material for wind turbine blades.

Muhammad Fudhail, Sofiyan Mohamed [4], This research has already compared three different designs to see how well they perform in terms of aerodynamics. This is the ideal specification to apply to wind turbine design with a 45° blade angle and 100cm length, according to one of the studies.

Vedulla Manoj Kumar and all [5], For the design and modeling of HAWT blades in this research report, Pro-E software was employed. Ansys Workbench software is used to perform the analysis. When compared to other epoxy glass materials, the static analysis findings show that the epoxy carbon material has the least deformation and the best performance (strength and hardness).

Er. Bharat Ankur Dogra, Dr. T.K. Jindal [6], It examines numerous design aspects and elements that influence wind turbine blades. An efficient blade shape is defined by aerodynamic load, according to a theoretical study on blade design. Airfoil portions of increasing width, thickness, and twist angle approaching the hub are required for optimal efficient sizing.

O.A.Abdul_Azim and all [7], For the same angle of attack =13°, optimized findings show that the output voltage and power [34 Watt-5.2 V average 4m/s] for the geared component can be produced, which is comparable to the normal drive gearless [144 Watts - 24.88 v on average 4m/s]. A geared machine's intrinsic mechanical friction loss has also been established, which is a clear advantage over mechanical gears for wind power applications.

Ale. Mishthauthaut kir t au au [8] On the one hand, chakras that are regularly regulated and stable are conducive to these viruses in every manner. On Khushlav, as a member of the wind, as friendly to the wind as I am, as joyful as I am, as an effective and healthy member of the wind for the windy season. It's the concept that matter has the power to change state, then thrive and flourish.

Peter J. Schubel, Richard J. Crossley [9], Aerodynamic calculations based on the specified parameters and the performance of the selected aerofoils define an effective blade shape, according to a thorough examination of blade design. Aesthetics merely plays a minor role. Aerofoil pieces of increasing width, thickness, and turning angle towards the hub are used to get the most efficient sizing. Physical principles constrain its broad shape, and it is unlikely to change. However.

C.M. Vivek, P and All [10], When compared to standalone vertical and horizontal axis wind turbines, combined vertical and horizontal axis wind turbines boost efficiency and production volume while reducing the area required by mounting vertical and horizontal wind turbines at the same time will do it Tower.

I.3. HISTORICAL DEVELOPMENT:

People have been using wind to move their sailboats for thousands of years, but the use of wind for mechanical and electrical purposes is the most important portion of the history of wind turbines.

Figure I. 1: Sailboat type.

Heron of Alexandria, a Greek engineer, was the first to use wind for mechanical purposes. He was the first to employ a wind-driven wheel to power a machine in the first century AD. Wind wheels were used to mill flour and corn, as well as pump water, in the Sistan area of Iran from the seventh to ninth centuries AD. By 1000 AD, windmills were being utilized in China for a different purpose: pumping seawater to manufacture salt.

Figure I. 2: Old windmills (Iran).

Vertical windmills were first employed to grind flour in northern Europe towards the end of the twelfth century, and they later became popular throughout Europe.

Figure I. 3: Old windmill (Netherland)

Professor James Blyth was the first to deploy wind turbines for energy-generating in Scotland in 1887. He put this wind turbine on his holiday cottage's lawn and utilized it to charge the battery. The wind turbine was initially constructed in the United States a year later,

by inventor Charles Brush. This inventor used this turbine to power his Ohio mansion with electricity (Fig I. 4).

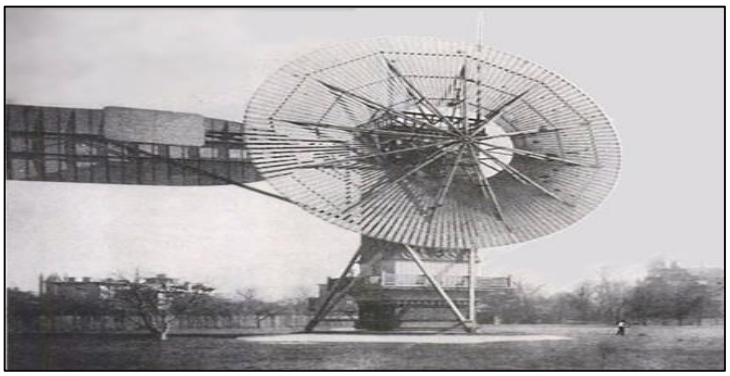

Figure I. 4: Charles Brush wind turbine US- 1888

I.4.WIND TURBINES:

A wind turbine is a device or equipment that converts wind kinetic energy into electrical energy.

I.4.1. Wind turbine components:

The rotor blade, gearbox, generator, nacelle, tower, and foundation are the six basic components of a wind turbine. Figure I.5 depicts the main components.

- ✓ **The nacelle:** The major components of a wind turbine, including gearbox and electric generator, include.
- ✓ **The tower:** Carries the nacelle and rotor. In general, having a taller tower is an advantage, as the wind speed increases farther away from the ground.
- ✓ **The rotor blades**: Capture wind power and transfer its power to the rotor hub.
- ✓ **The generator:** converts the mechanical energy of the rotating shaft to electrical energy.
- ✓ **The gearbox:** increases the rotational speed of the shaft for the generator.
- ✓ **Foundation:** Prevents the wind turbine from blowing over in high winds.

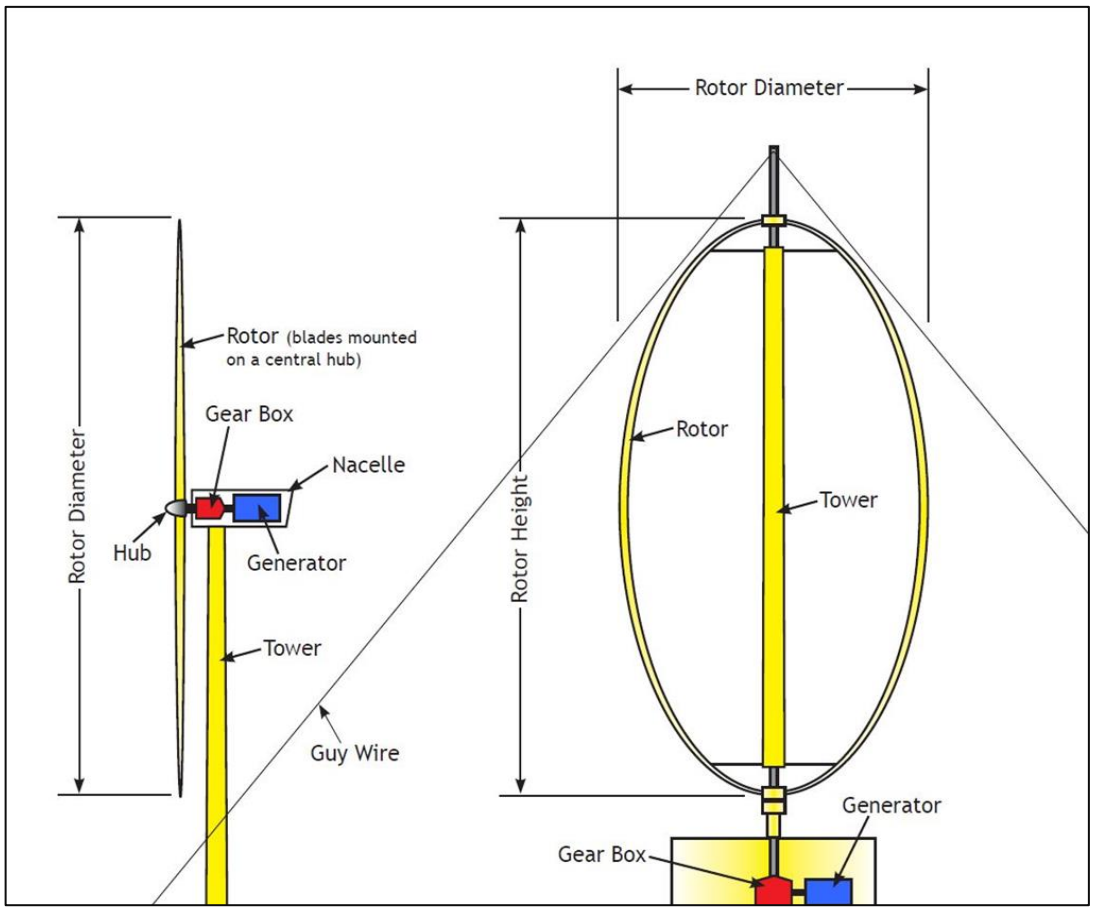

Figure I. 5: Wind turbine components

Figure I. 6: Inside mechanical components of the nacelle

Figure I. 7: Wind turbine foundation

I.4.2. Wind turbine types:

Wind turbines are classified into two general types: horizontal axis (HAWT) and vertical axis (VAWT). A horizontal axis wind turbine has its blades rotating on an axis

parallel to the ground but the vertical one his blades rotating on an axis perpendicular to the ground.

Figure I. 8: Vertical Axis Wind Turbine (VAWT) **Figure I. 9:** Horizontal Axis Wind Turbine (HAWT)

I.4.2.1. Horizontal wind turbine types:

Horizontal axis wind turbines are the most commonly used turbines, this type having a main rotor shaft and an electric generator at the top of a tower. Small turbines are guided in the direction of the wind by a small wind vane, while larger turbines use wind sensors with yaw systems. Most of these types have a gearbox that converts the slow rotation of the blades to the faster rotation. Some generators are optimized with a slower rotational speed, with this type of generator being attached directly to the rotor without a gearbox.

Figure I. 10: Horizontal Axis Wind Turbines (HAWT)

Depending of the relative position of the rotor and wind direction, two types of horizontal wind turbines can be distinguished:

I.4.2.1.1. up-wind turbine:

The primary disadvantage of this design is that the blades must be sturdy, rigid, and far apart to avoid hitting the tower during high winds. Furthermore, to endure the wind, these rotors require a Yaw system. This is the design of the vast majority of wind turbines.

I.4.2.1.2. down-wind turbine:

The rotor is on the flow side of the tower in a downwind turbine. One advantage is that the rotor follows the wind's direction without the use of a yaw system. Because there is no chance of the blades impacting the tower, rotor blades can be more flexible than upwind designs. They can also minimize the stress on the tower during high wind speeds, allowing the blades to be manufactured lighter than upwind designs. the main disadvantage is that when the blades travel through the area of the wind behind the tower, the wind power is unstable. As a result, as the rotor passes behind the tower, power may be reduced. The situation of huge turbines exemplifies this issue.

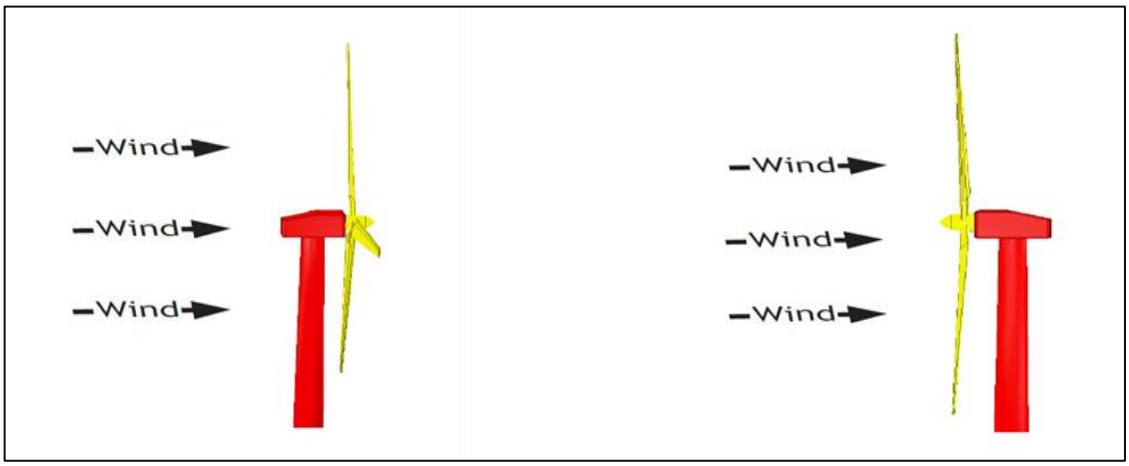

Figure I. 11: Down- wind and Up-wind of wind turbine

I.4.2.2. Vertical axis wind turbines (vawt):

These turbines contain a rotor shaft and blades that revolve perpendicular to the ground, requiring no rotation to follow the wind direction. The gearbox and generator can also be located close to the ground. Turbines situated at ground level have the advantage of being easy to maintain and can be erected in places like roofs. These designs, on the other hand, create very little energy, which is a significant disadvantage.

I.4.2.2.1. Darrieus wind turbines:

The Darrieus is a type of vertical wind turbine named after Georges Darrieus, a French inventor. This form has an airfoil design that moves by using the lift forces of the wind, similar to aviation wings. This vertical model does not self-start and requires a motor to create speed before it can generate substantial torque. It is efficient, but it produces a lot of torque ripple and cyclical stress on the tower, which makes it unreliable. The torque ripple is minimized when three or more blades are used, resulting in increased rotor solidity. Guy

wires are no longer used to support newer Darrieus turbines, which instead feature an exterior superstructure attached to the top bearing.

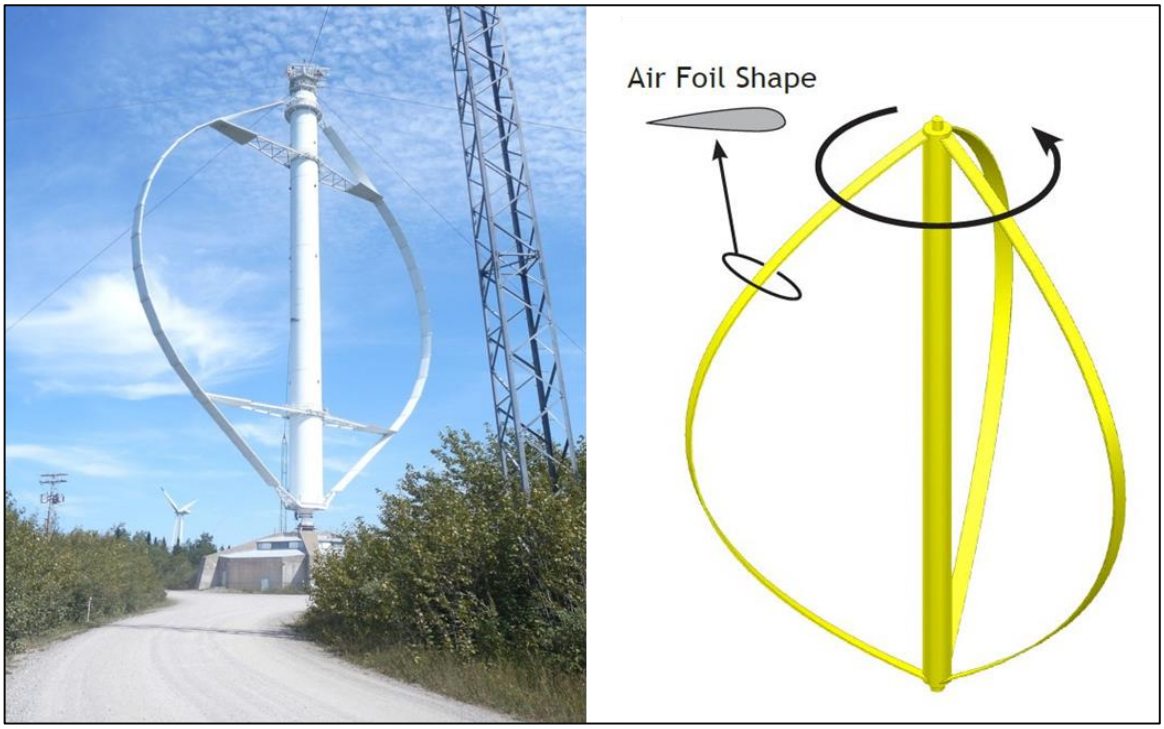

Figure I. 12: Darrieus turbine holded by guy-wire. **Figure I. 13:** Darrieus turbine schematic.

I.4.2.2.2. Giro mill wind turbine:

This type of turbines called also H-rotor or H-bar. In which the blades of Darrieus design are replaced with straight vertical blades attached to the central tower with horizontal supports.

Figure I. 14: Giromill wind turbine

I.4.2.2.3. Savonius wind turbine:

This type of turbines contains at least two scoops (half cylinder), and usually placed on truck and bus roofs.

Figure I. 15: Savonius wind turbine.

I.4.3. Wind turbine blades materials & properties:

I.4.3.1. Materials in wind blades:

E-glass and polyester resins are the most often utilized fibers and their matrix. The amount of fiber FVF in the resins impacts the composite's strength, depending on the production procedures used. When a certain amount of fiber is added to a composite, the mechanical qualities start to suffer since there aren't enough resins to transfer the load to the fiber. Normal hand layup procedures can achieve FVF of roughly 30-35%, whereas advanced processes such as SCRIMP and vacuum infusion employing prep lugs can achieve FVF of up to 70%. [11]

I.4.3.1.1. Polyester resin:

The orthotropic resin and the isotropic resin are two forms of polyester that have superior water resistance. Polyester has a short storage life. If the producer does not add other chemicals (such as catalysts, accelerators, and additives), it is usually required when used for molding. Because of its chemical resistance, it becomes brittle when subjected to shock

loading, making it ideal for small-scale wind turbine blades. Other resins, on the other hand, fight fiercely for larger wind turbine blades.

I.4.3.1.2. aramid:

Aramid is a material with high specific strength. It has a number of qualities that make it appropriate for a variety of applications, including boat building. It has a broad strength equivalent to E-glass fiber; however, it is more impact resistant. Aramid's disadvantages include its sensitivity to water intrusion, UV deterioration, and insect collision because of its high impact resistance. Because of its fatigue resistance capacity, it is also high enough to manufacture a powerful wind blade material. [11]

I.4.3.1.3. carbon fiber:

Carbon fiber, a high modulus reinforcement material, was originally predated by boron fibers, and the cost of boron has been reduced as a result of its substitution with carbon fiber. Though they have the same tensile strength as glass fiber, their modulus might be five times greater. The important advantage is that the goal of reinforcing is to make the structure stiffer. [10]

I.4.3.2. Materials properties:

I.4.3.2.1. Elastic properties:

Modern wind turbine blades are three-dimensional structures constructed of a variety of materials, and the elastic properties and thermal–physical constants of the materials, such as the thermal expansion coefficient, determine the damage that develops in a blade. As a result, the stress field is influenced by the materials' elastic characteristics. The elastic properties of isotropic materials are the Young's modulus, E, and the Poisson's ratio. Orthotropic materials have different elastic properties in different directions, such as composite laminates with aligned continuous fibers. [14]

Table I.1. Classification of materials used in wind turbine blades

Isotropic materials	Orthotropic materials
Adhesive	Glass fiber/polyester composites
Steel	Carbon fiber/epoxy composites
Polymer foam	Wood (e.g. birch or balsa)
Gelcoat	Bamboo

Table I.2: Aramid (Kevlar) fiber properties

	Kevlar 29 High toughness	Kevlar 49 High Modulus	Kevlar 149 Ultrahigh Modulus Tensile
Tensile Strength	3.6 Gpa	3.6-4.1 Gpa	3.4 Gpa
Young's Modulus	83 Gpa	131 Gpa	179 Gpa
Elongation at Break	4%	2.8%	2%

Table I.3: Carbon fiber properties

	Standard modulus	Intermediate modulus	High modulus
Tensile Strength	3450-4830 MPa	3450-6200 MPa	3450-5520 MPa
Young's Modulus	220-241 GPa	290-297 GPa	345-448 GPa
Elongation at Break	1.5-2.2%	1.3-2.0%	0.7-1.0%

I.4.4. Wind turbine blade airfoils:

Airfoil families have been used to construct wind turbine blades. In HAWT, NASA LS, NACA 44xx, and NACA 63-xxx were commonly used. Roughness effects caused by leading-edge contamination, on the other hand, degrade their performance [12]. The NACA airfoil series in four digits was created geometrically using analytical equations that define the camber (curvature) of the mean-line (geometric centerline) of the airfoil section, as well as the thickness distribution of the section throughout its length. It's thought that the 6-digit airfoil series designs are more theoretical than geometrical and that changing them to include certain variables makes them more intricate.

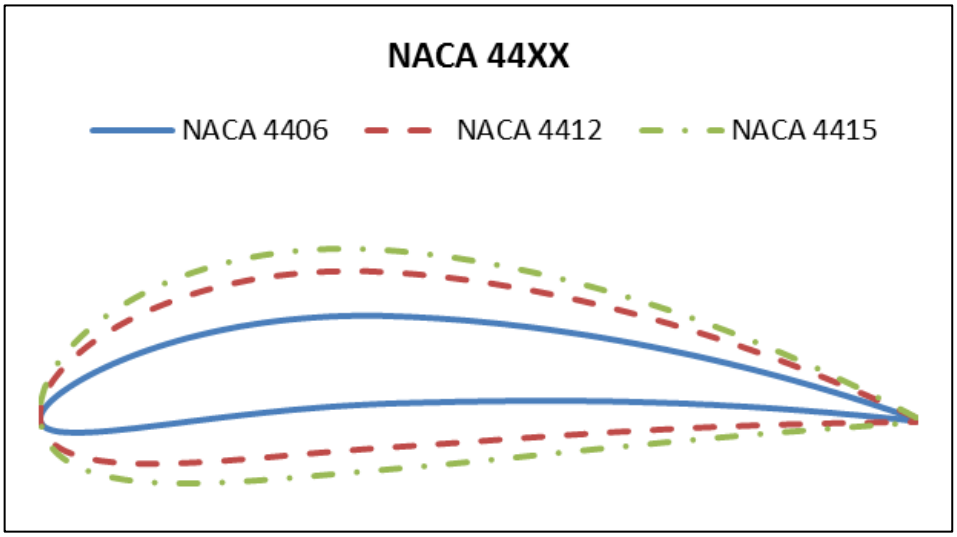

Figure I. 16: NACA 44xx airfoil geometrical construction [12].

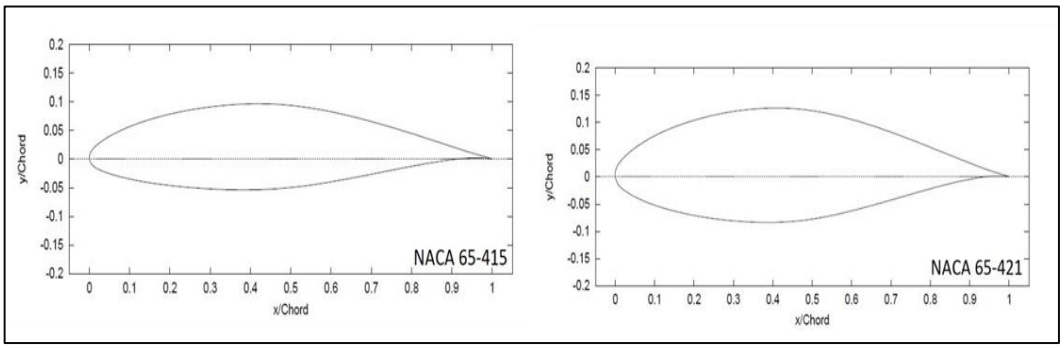

Figure I. 17: NACA65-415 & NACA65-421 Airfoils [12].

With the help of Tangler and Somers, the National Renewable Energy Laboratory (NREL) was able to overcome energy losses when it began developing various series of airfoils for wind turbines in the 1980s.

It uses the Eppler airfoil design and analysis programme to create nine airfoil families for various rotor diameters. The performance requirement for the airfoil family is to maximize the life coefficient, which is essentially unaffected by roughness effects. The NREL airfoil families have improved annual energy production in numerous types of wind turbine blades, according to [12].

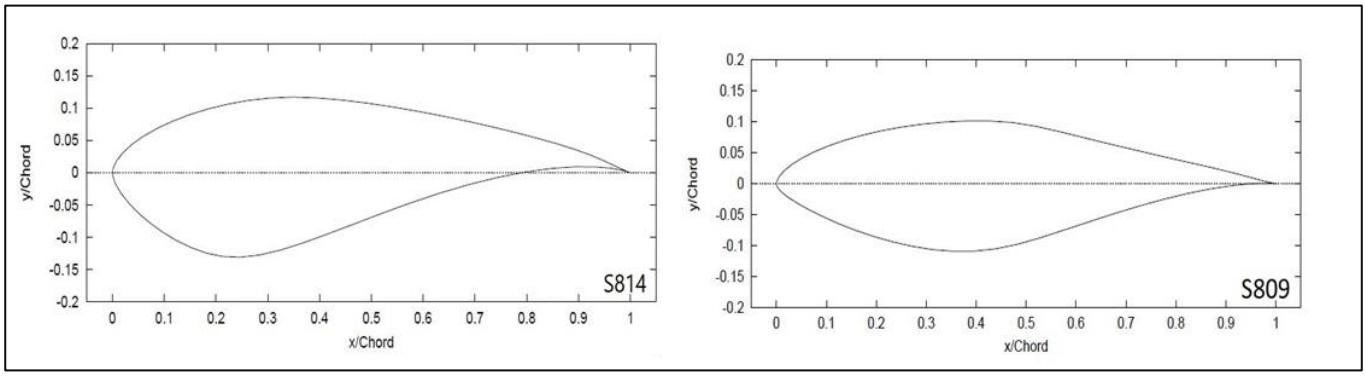

Figure I. 18: S814 & S809 NREL Airfoils [12].

In the mid-1990s, RISO designed three airfoil families, Riso-A1, Riso-P, and Riso-B1, for rotor sizes ranging from 600 kW to MW. The direct method of a numerical optimization algorithm of a B-spline representation of the airfoil form is used to build the RISO-A series. In the RISO airfoil series, this approach was found to be insensitive to leading edge roughness. [12].

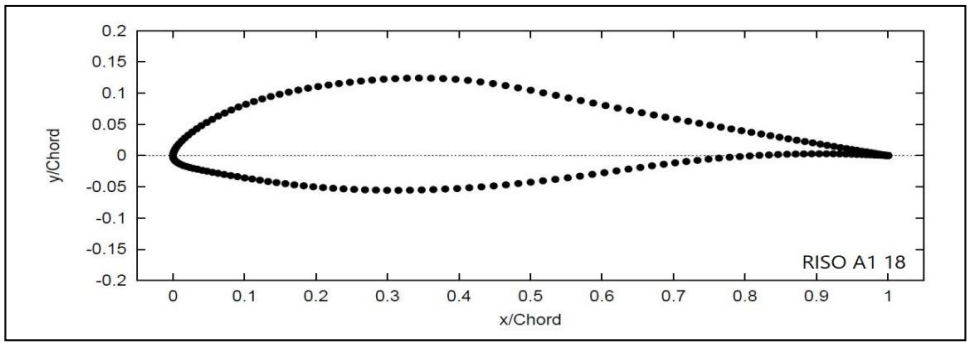

Figure I. 19: A1-18 RISO Airfoils [12]

Deft University of Technology created DU airfoils (DUT), The maximum relative thickness of the DU-airfoils is from 15% to 40% chord. The XFOIL code was used to create the first designs. Since 1995, the airfoils have been designed using the computer program RFOIL, which is a modified version of XFOIL with enhanced prediction around the maximum lift

coefficient and the ability to anticipate the influence of rotation on airfoil properties. Gurney flaps, trailing edge wedges, vortex generators (vg), and trip wires have been measured and their effects on the airfoil characteristics of various DU-airfoils are provided. In addition, for leading edge separation, a relationship between the thickness of the airfoil leading edge and the angle-of-attack is given.

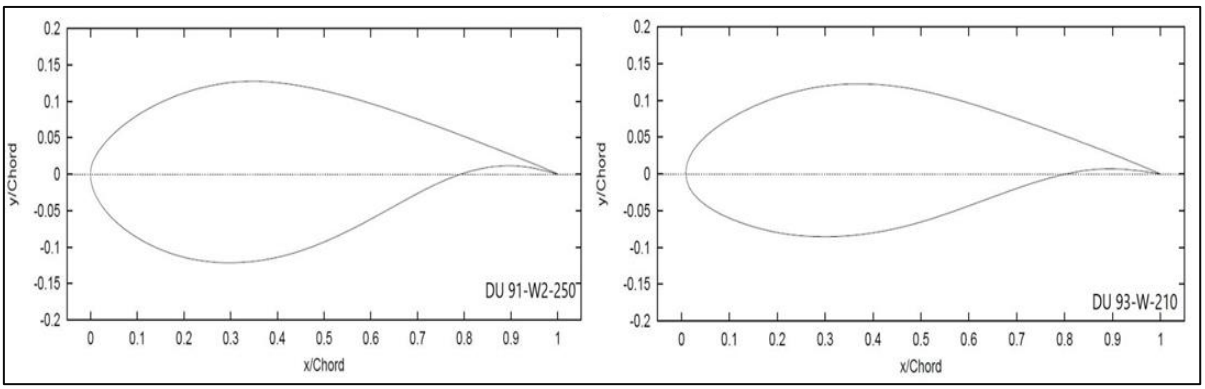

Figure I. 20: DU91-W2-250 and DU93-W-210 Airfoils [12]

I.4.6. WIND TURBINE APPLICATIONS:

Wind turbine is one of the most useful tools to harness wind energy. Following are some of the most important uses of wind turbines:

I.4.6.1. Generate Electricity:

Electricity is generated by wind energy. Electricity is traditionally generated using nonrenewable resources such as coal and petroleum. The heat energy created by burning objects is used to generate electrical energy. This energy is also used to power home appliances and is used commercially to power refrigerators, air conditioners, and television sets. Non-renewable commodities like coal and petroleum, on the other hand, emit massive volumes of damaging waste in the form of toxic gaseous wastes like carbon monoxide, carbon dioxide, and methane. This results in air pollution, which has a significant negative impact on the natural environment's long-term sustainability. This is avoided by using wind power. Turbines are one of the most effective ways to transform wind energy into electricity. The energy is tapped by the winds and turned into electrical energy when the turbines rotate. This energy can be used to power tidal power plants and business equipment in homes and offices as an alternate source.

I.4.6.2. Powered Vehicles:

Wind turbines are the main proponents for generating electricity, which is then utilized to power turbines and assist in the propulsion of motorized vehicles. Through the various engine belts and rotators, the wind energy created by the movement of the turbines is transferred to mechanical energy. The mechanical energy so created aids in vehicle

propulsion, therefore improving the energy conversion process. As a result, because the process uses renewable energy sources, the risk of contamination or effluent discharge is greatly reduced.

I.5.CONCLUSION:

Wind power is probably the solution to our energy demands. It has great potential and is easy to manage. All you have to do is build the turbine and everything else is going to be free. As long as the wind blows, wind turbines can harness the wind to generate electricity. Wind power only makes up a small percentage of the electricity that is produced for now. Unlike coal, wind turbines do not create greenhouse gases and are a completely renewable source. Many people believe that wind power may soon be our main source of energy. Although wind turbines can cause complaints and death of wildlife, it may be the energy solution we are looking for.

Chapitre II

Aerodynamic of wind turbine blade

II.1. INTRODUCTION:

The kinetic energy in the wind is converted into mechanical energy in a shaft, and then into electrical energy in a generator. If the wind speed can potentially be lowered to zero.

II.2. Wind turbine blade aerodynamics 2D:

Many aerodynamic models assume that the flow at a particular radial position is two-dimensional and a 2-D airfoil because wind turbine blades are long and slender structures with a much lower spanwise velocity than the component streamwise velocity. The data can be used in the following way. Two-dimensional flow contains a plane, and the velocity component in the z-direction is zero if the plane is characterized using the coordinate system given in Fig.II.1.

To create a two-dimensional flow, an airfoil must be extruded into an infinite-span wing. On a real wing, the chord and twist change along the span, and the wing begins at a hub and ends at a tip, but Prandtl has shown that for long, slender wings, such as those found on modern gliders and wind turbines, local 2-D data for the forces can be used if the angle of attack is corrected appropriately with the trailing vortices behind the wing [17]. Even though it is difficult to grasp, 2-D aerodynamics is clearly of practical interest. The leading-edge stagnation point in the 2-D flow across an airfoil is seen in Figure II.1. The flow's responding force F is split into two directions: perpendicular to the velocity V and parallel to V. The former is referred to as the lift (L), while the latter is referred to as the drag (D) (see Figure II.2).

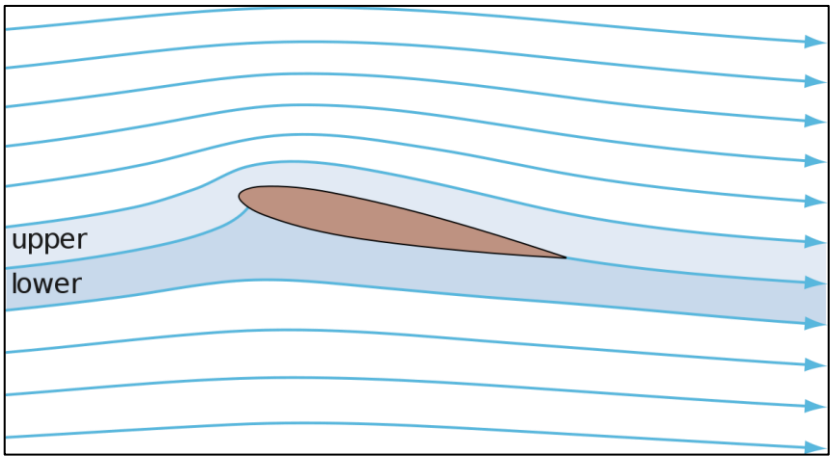

Figure II.1: Schematic view of streamlines past an airfoil.[18]

II.2.1. CHARACTERISTIC AND PARAMETERS:

II.2.1.1 Power coefficient:

The power coefficient is the most critical variable in wind turbine aerodynamics; because the wind speed cannot be lowered to zero, the power coefficient is the ratio of real power to maximum available power, as provided by the equation above. In fact, reducing wind speed by nearly two-thirds allows for a theoretical maximum Cp, Cpmax = 0.593, as defined by Betz theory.[17]

The real power C_p was much lower than its theoretical limit and ranging from 30 to 40%, but modern wind turbines operate close to maximum limit, with C_p up to 0.5.

$$C_{P=\frac{P}{\frac{1}{2}\rho AV^3}} \quad \text{II.1}$$

To fully explain the forces, the moment M about a point in the airfoil must also be known. This point is frequently seen on the leading edge's c/4 chord line. When the airfoil in Figure II tends to turn, the moment is positive. A moment coefficient is defined as: 2 clockwise (nose up) and a moment coefficient is defined as:

$$C_m = \frac{M}{\frac{1}{2}\rho V_\alpha^2 C^2} \quad \text{II.2}$$

II.2.1.2 Trust coefficient:

The thrust is the force in the streamwise direction resulting from the pressure drop over the rotor.

$$T = \Delta p.A \quad \text{II.3}$$

Where $A = \pi.R2$ is the area of the rotor and Δp is the pressure drops over the rotor.

The thrust coefficient is another important dimensionless number in wind turbine aero dynamics, it is defined as:

$$C_T = \frac{T}{\frac{1}{2}\rho AV^2} \quad \text{II. 4}$$

II.2.1.3 Tip-Speed Ratio:

The Tip-Speed Ratio λ is defined as:

$$\lambda = \frac{U}{V} \quad \text{II. 5}$$

U is the speed of rotor at the tip of blades: $U = \omega.R$, where R is the blade radius and ω is the rotational velocity in (radians/second), V is the wind speed.

II.2.1.4 Lift and Drag Coefficients:

The wind turbines blades generate a lift force due to their shape like airplane wings. This force is a net result of low pressures in the more curved side and high pressure in the other side of airfoil.

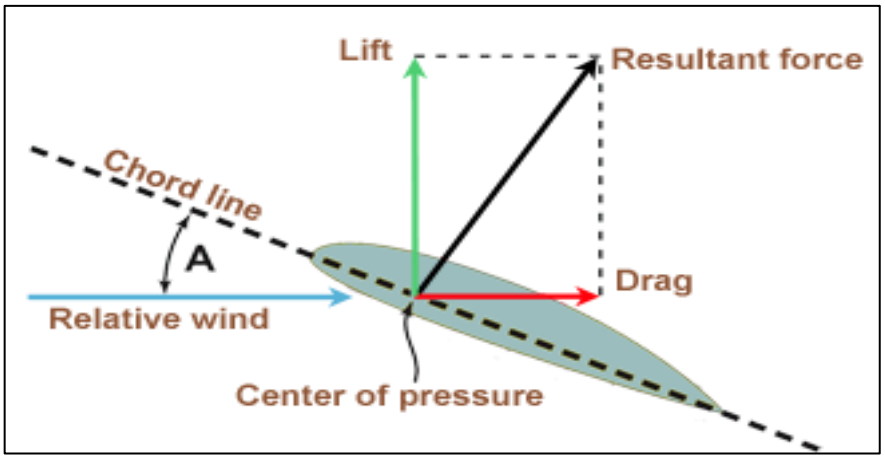

Figure II.2: Lift and Drag Forces

The lift force is always perpendicular to the airflow direction and grows as the blade gets closer to the wind. The lift force drops to zero at a very large angle of attack, indicating that there is an ideal angle of attack for maximal lift.

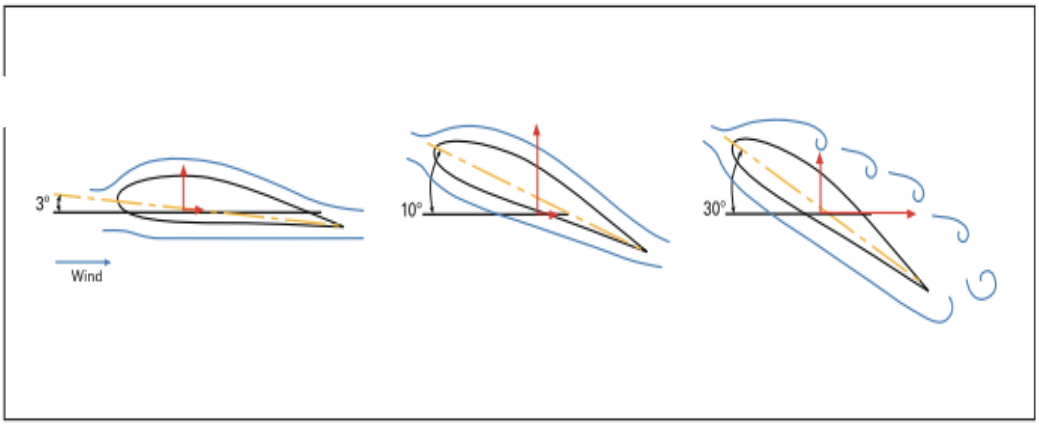

Figure II.3: Lift forces at low, medium and high angels of attack.

Another force parallel to the air flow: Drag. This force increases with angle of attack and reaches the maximum value at high angles. Lift and drag coefficients are defined as:

$$C_L = \frac{L}{\frac{1}{2}\rho A W^2} \qquad \text{II. 6}$$

$$C_D = \frac{D}{\frac{1}{2}\rho A W^2} \qquad \text{II. 7}$$

Where W is the relative wind as experienced by the blades. This speed is done by the relation below:

$$\overrightarrow{W} = \vec{V} - \overrightarrow{U} \qquad \text{II.8}$$

II.2.2. BLADE ELEMENT MOMENTUM METHOD:

The blade element theory combines the two approaches to understanding how a wind turbine works. The first way involves using motion theory, also known as disc actuator theory, which is a mathematical model of an ideal actuator disc. The motion balance on a revolving annular stream tube traveling through a turbine is investigated using motion theory. The blade element theory, which defines local aerodynamic processes that occur on the blade, is the second way. The aerodynamic forces generated by an airfoil are investigated using blade element theory. Then, using these two procedures, a set of equations can be generated. It is possible to solve the resulting equation iteratively.

There are two iterative variables that are axial and radial induction factors, in BEM theory. These variables can be defined as follows.

$$a = \frac{1}{4\,sin^2\,\emptyset/(\sigma C_N)+1} \qquad \text{II.9}$$

$$a' = \frac{1}{4\sin\emptyset\cos\emptyset/(\sigma C_T) - 1} \qquad \text{II.10}$$

Where, $\emptyset$ is the inflow angle, $C_T$and $C_N$is the tangential and normal force coefficient respectively, σ is the solidity which is defined as the ratio of the planform area of the blades to the swept area. It can be expressed as follows:

$$\sigma = \frac{cB}{2\pi r} \qquad \text{II.11}$$

Where, c is the chord length, B is the number of blades and r is the disk radius.

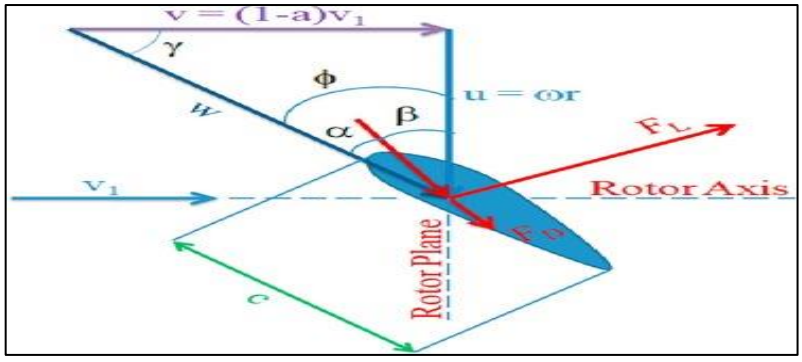

Figure II.4: Velocity component in the rotor plane. [19]

The velocity component in the rotor plane is shown in Fig.II.4. The inflow angle can be calculated by first guessing the axial and radial induction factors. The angle of attack,

defined as the angle between the chord line of the airfoil and the relative wind speed, can then be calculated using the equation below:

$$\theta = \theta p + \beta \quad \text{II.12}$$

$$\alpha = \emptyset - \theta \quad \text{II.13}$$

Where β is a twist angle of the blade, θp is a pitch angle of the blade, θ is the combination of the twist angle β and the pitch angle θp. After the calculation of the angle of attack, the lift and drag coefficient of the airfoil can be obtained from the lift and drag curves of the airfoil. By using these force coefficients, new induction factors can be calculated and compared to the initial induction factors. When the maximum value of the $\boldsymbol{\Delta a}$ and $\boldsymbol{\Delta a'}$ is below the convergence criterion ε, it means that the iteration converges. Then, the next element can be calculated.

The flow diagram, which is used to solve iteratively for Axial Induction Factor and the Radial Induction Factor solution of BEM theory is shown in Fig.II.5.

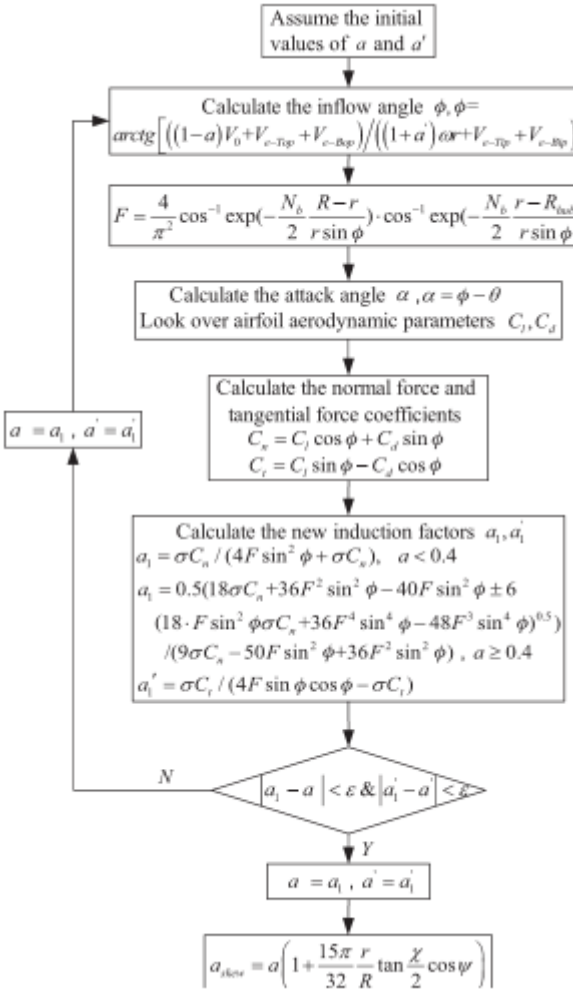

Figure II.5: Flow Diagram of the Iteration Process Used to Solve for Axial Induction Factor and the Radial Induction Factor.

II.3. Wind turbine blade aerodynamics 3D:

This section discusses the 3-D wing's flow quality and how the upstream flow and angle of attack are affected by spanwise lift distribution. The wing is a finite-length beam with airfoils as cross sections, resulting in a pressure difference between the lower and upper sides, which causes lift. Where air moves from the bottom up, there are leaks at the tips. As a result, the streamline running over the wing is deflected inwards, while the streamline flowing under the wing is deflected outwards. As a result, the tangent velocity at the trailing edge increases. (See Figure II.5 and II.6)

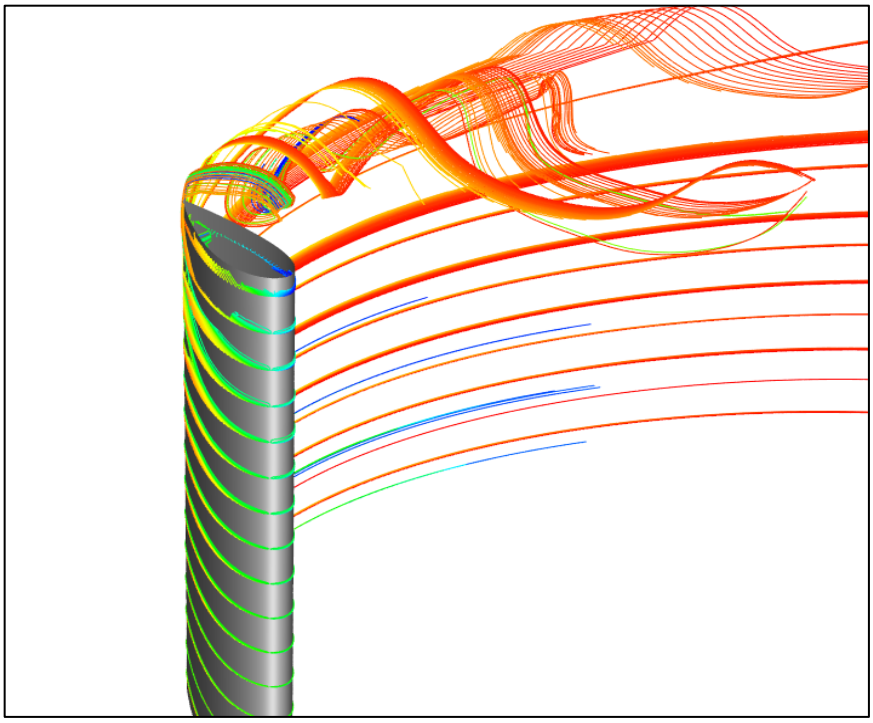

Figure II.5: Streamlines flowing over and under a blade

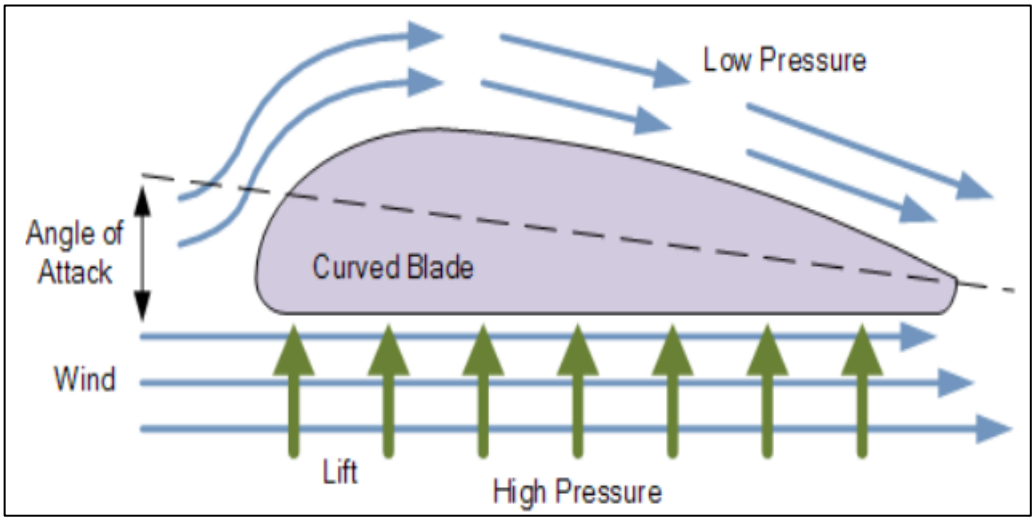

Figure II.6: Velocity vectors are seen from behind a wing.

II.3.1 Vortex System behind a Wind Turbine:

The rotor of a horizontal-axis wind turbine consists of a number of blades, which are shaped as wings. If a cut is made at a radial distance, *r*, from the rotational axis as shown in Figure II.7. The local angle of attack α is given by the pitch of the airfoil θ; the axial velocity and rotational velocity at the rotor plane denoted respectively by Va and V_{rot} (see Figure II.7):

$$\alpha = \varphi - \theta \qquad \text{II.14}$$

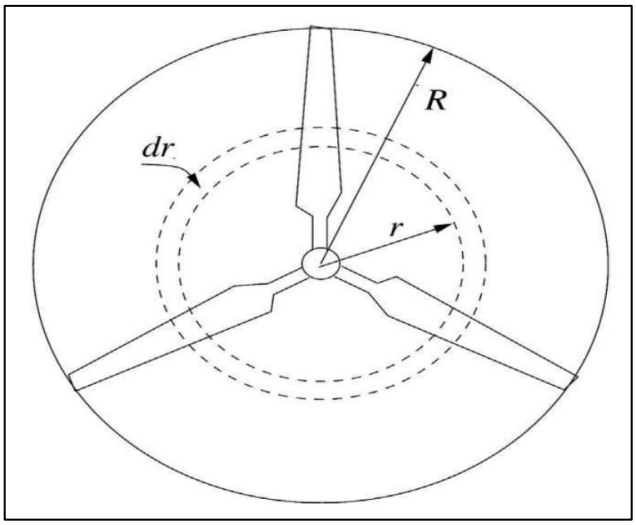

Figure II.7: Rotor of a three-bladed wind turbine.

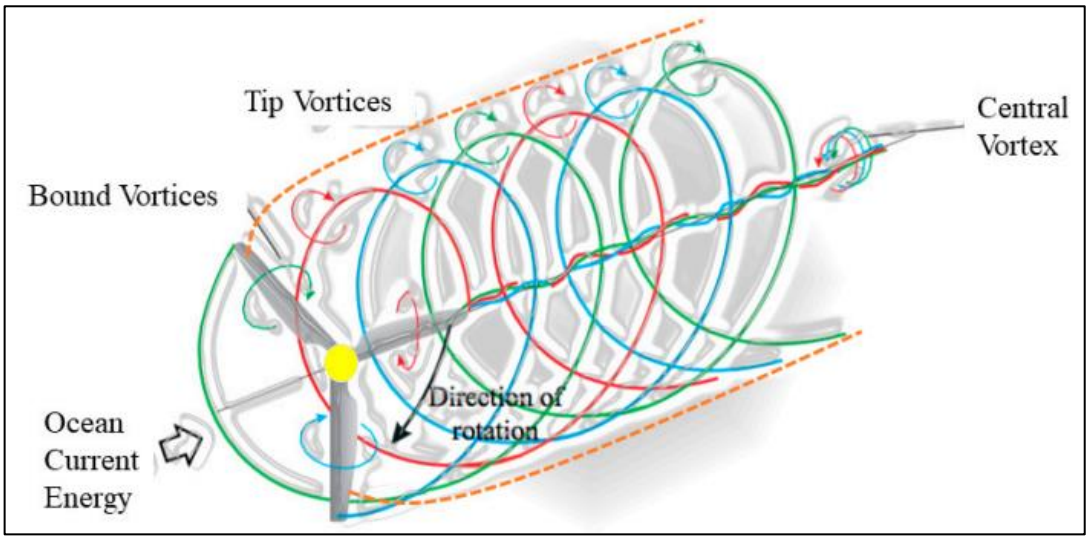

Figure II.8: Schematic drawing of the vortex system behind a wind turbine.[20]

Where the flow angle ∅is found as:

$$\tan \emptyset = \frac{V_a}{V_{rot}} \qquad \text{II.15}$$

A vortex system similar to the linear translating wing must exist in a horizontal-axis wind turbine because it is made up of rotating blades. The free vortices' vortex sheet is positioned in a helical pattern behind the rotor. The powerful tip vortices are found at the rotor wake's edge, whereas the root vortices follow a straight course along the rotor's axis, as seen in FigureII.8. On a wind turbine, the vortex system produces an axial velocity component in the opposite direction of the wind and a tangential velocity component in the opposite direction of the rotor blade rotation. The axial induction factors a specifies the induced velocity in the axial direction as a V, where V is the undisturbed wind velocity. The induced tangential velocity in the rotor wake is specified through the tangential induction factor a' as $2a'\omega r$. Since the flow does not rotate upstream of the rotor, the tangential induced velocity in the rotor plane is thus approximately $a'\omega$ r. ω denotes the angular velocity of the rotor and r is the radial distance from the rotational axis. If a and a' are known, a 2-D equivalent angle of attack could be found from equations II.13 and II.14, where:

$$V_a = (1- a)\, V \qquad \text{II.16}$$

And

$$V_{rot} = (1+ a')\, \omega r \qquad \text{II.17}$$

It is equally simple to determine the force distribution provided the lift and drag coefficients (CL) and (CD) for the airfoils applied along the blades are also given. By integrating this distribution along the span, global loads such as power output and root bending moments of the blades can be obtained. The Blade Element Momentum method is used to calculate the induction factors a and a', as well as the loads on a wind turbine. It is also feasible to use the vortex approach and build the vortex system as indicated in Figure 8, then compute the induced velocities using the Biot-Savart equation.

II.4. CONCLUSION:

Lift is lowered for a three-dimensional wing at the same geometric angle of attack as a two-dimensional wing, and local lift has a component in the direction of onset flow, which is known as induced drag. The downwash produced by the 3-D wing's vortex mechanism is responsible for both effects. Lifting line theory posits that three-dimensionality is limited to downwash, that is, the spanwise flow is still tiny in comparison to the stream velocity, and that 2-D data can be employed locally if there is an assault. The downwash changes the geometric angle. For long, narrow wings, such as gliders or wind turbines, this assumption is feasible.

Chapitre III

Results and discussion

III.1. INTRODUCTION:

In this study, we used QBlade and Ansys-Fluent to forecast the aerodynamic performance of a 10kw horizontal wind turbine with a rotor diameter of 6 m and NREL S809 as an airfoil. QBlade (Software under General Public License) is used to design the turbine and acquire aerodynamic performance optimization and analysis. QBlade uses the Blade Element Momentum (BEM) approach for wind turbine simulation and is combined with the XFOIL airfoil design and analysis. After that, using CFD methodologies, the aerodynamic performance is estimated (Fluent commercial software). Finally, the Qblade findings are compared to the power and torque coefficients curves of the turbine produced from the 3D CFD data.

III.2. BLADE SHAPE DESIGN FOR OPTIMUM ROTOR:

When an ideal rotor is design, the effect of wake rotation is taken into design. The blade shape optimization for ideal rotor includes wake rotation except drag (CD = 0) and tip losses (F = 1). The power coefficient depends on the angle of the inflow angle, ø. The power coefficient can be obtained from the following equation:

$$C_P = \left(\frac{8}{\lambda^2}\right)\int_{\lambda h}^{\lambda} \sin^2\emptyset\,(\cos\emptyset - \lambda_r \sin\emptyset)$$

$$(\sin\emptyset + \lambda_r \cos\emptyset)[1 - (C_d/C_l)\cot\emptyset](\lambda_r)^2 d\lambda_r \qquad \text{III.1}$$

Taking the partial derivative of the part of the integral for C_p and the derivative is set to equal zero.

$$\frac{\partial}{\partial\emptyset}\left[\sin^2\emptyset\left(\cos\emptyset - \lambda_r \sin\emptyset\right)\left(\sin\emptyset + \lambda_r \cos\emptyset\right)\right] = 0 \qquad \text{III.2}$$

The local tip speed ratio, inflow angle, chord length of the blade section can be calculated as the follows:

$$\lambda_r = \sin\emptyset\,(2\cos\emptyset - 1)/[(1 - \cos\emptyset)(2\cos\emptyset + 1)] \qquad \text{III.3}$$

$$\emptyset = (2/3)\tan^{-1}\left(1/\lambda_r\right) \qquad \text{III.4}$$

where λ_r is the local tip speed ratio, c is the chord length of the blade section, B is the number of the blade, C_l is lift coefficient at the angle of the attack, α which the angle is at the highest value of the ratio of the lift-drag coefficient.

For an ideal wind turbine blade design, the following steps are applied:

1. Determine the blade diameter.
2. Choose a design tip speed ratio

3. Select the airfoil type for wind turbine
4. Determine the angle of attack
5. Divide the blade to sections
6. Calculate the inflow angle for each section
7. Calculate the chord length for each section
8. Calculate the twist angle by using (5) for each section

We followed the processes previously outlined for an optimal wind turbine blade design, first deciding to design a 6 m blade diameter turbine. The NREL S809 airfoil, which is specifically built for wind turbines with small blades, was chosen. The tip speed ratio was set at 7. In the case of the NREL S809 airfoil, From QBlade software, the lift coefficient at 6° angle of attack, where the CL/CD ratio has the highest rate, was found to be 0.847. (Fig.III.3 & Fig.III.4). The blade section was separated into 11 sections. The inflow angle, chord length, and twist angle for each segment were then computed using the formula.

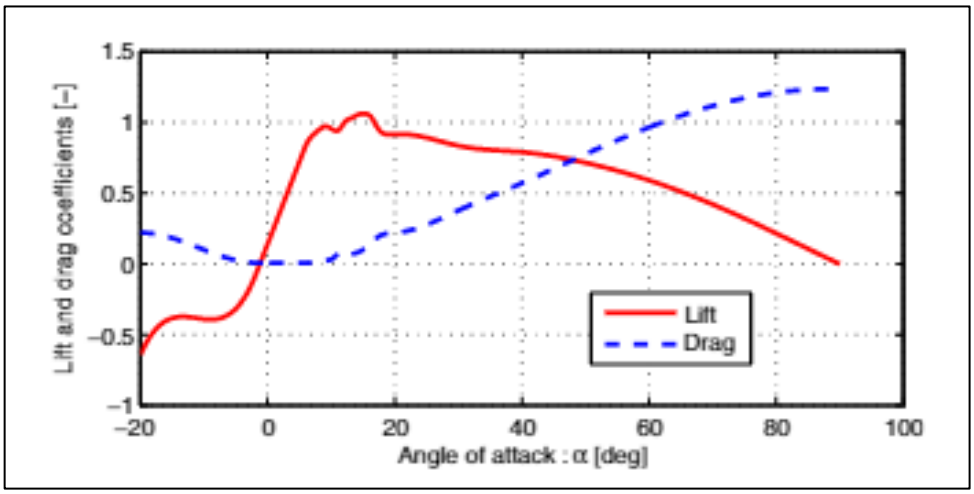

Figure III.1: C_L and C_d graph for NREL S809 airfoil.

The rotor blades parameter and the design parameter of wind turbine are listed in Tab.III.1 and Tab.III.2, respectively.

Table III. 1: The parameter of the rotor blades**.**

Blade parameters	values
Radius of blade (m)	6
Number of the blades	3
Airfoil type	S809
Chord length (m)	Listed in Tab.III.2
Twist angle (deg)	Listed in Tab.III.2

Table III. 2: Design parameter of blade.

Geometry of Blade				
Section	**Position (m)**	**Chord length (m)**	**Twist angle (deg)**	**Airfoil**
1	0,150	0,075	0	Circle
2	0,300	0,075	0	Circle
3	0,467	0,250	17,4	S809
4	0,783	0,376	11,1	S809
5	1,100	0,319	8,2	S809
6	1,417	0,273	5,2	S809
7	1,733	0,228	3,3	S809
8	2,050	0,195	1,9	S809
9	2,367	0,170	0,8	S809
10	2,683	0,150	0	S809
11	3,000	0,135	-0,6	S809

The NREL S809 airfoil has a maximum thickness of 21% at 39.5% chord, a maximum camber of 1% at 82.3% chord. The profile is shown in Fig. 4. Also blade model of turbine is shown in Fig.III.3.

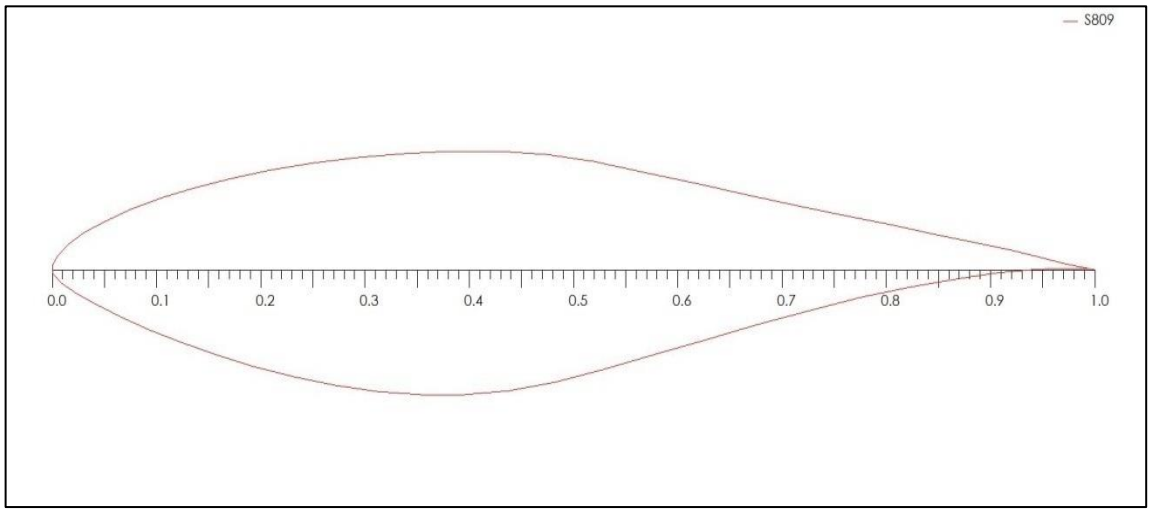

Figure III.2: NREL S809 airfoil profile

III.4. QBlade Analysis:

QBlade analyses were conducted on the turbine blade in the range of the tip speed ratio, λ from 3 to 10. In the analyses design the wind speed of 10 m/s was kept to be constant while the rotation of the rotor was varied with respect to λ. As results, the power and torque coefficients (Cp & Cm) values vs. various TSR graphics were obtained (III.8 & III.9).

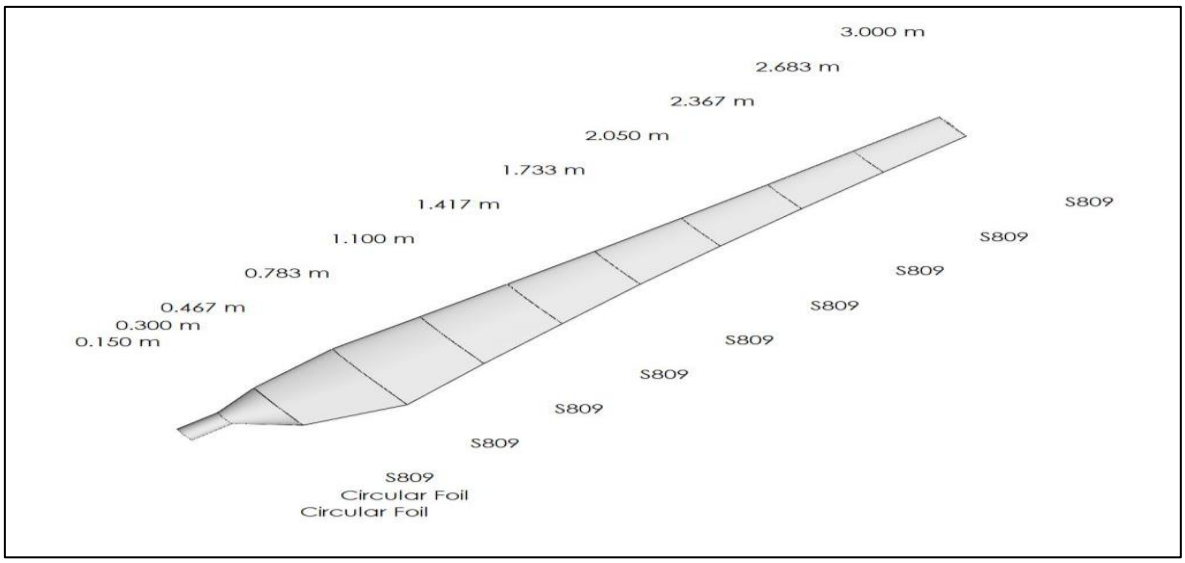

Figure III.3: Blade model of wind turbine using Qblade

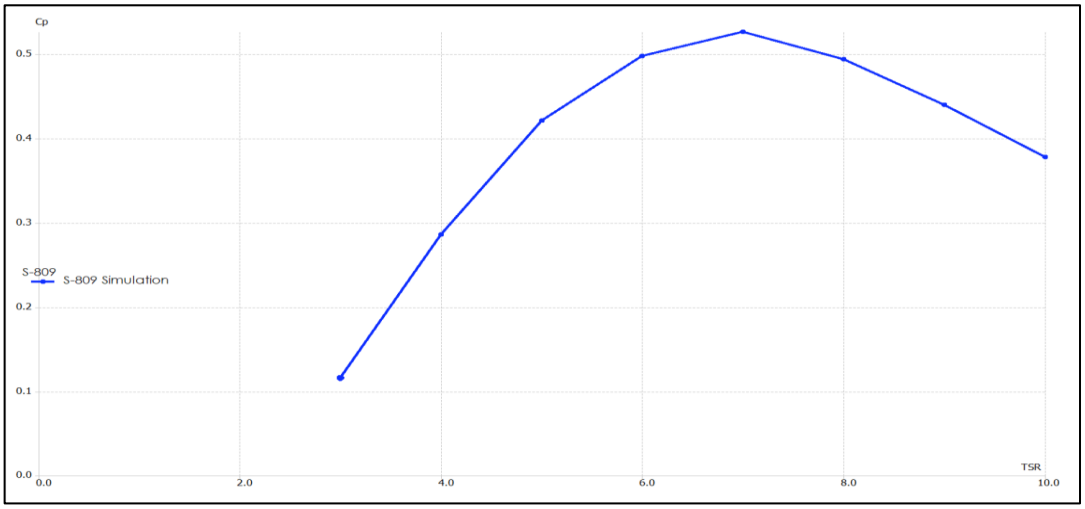

Figure III.4: The power coefficient versus tip speed ratio graphic using Qblade.

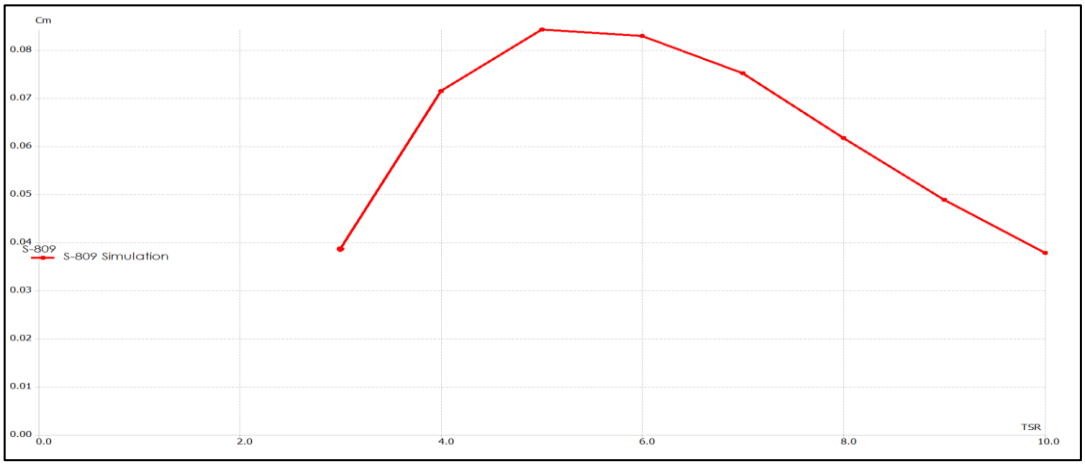

Figure III.5: The Torque coefficient versus tip speed ratio graphic using Qblade.

III.5. 3D CFD Analysis:

Numerical simulations for aerodynamic performance of wind turbine were carried out by using ANSYS-Fluent, which is commercial software for CFD analysis based on the finite volume method. In CFD analysis, SST k-ω turbulence module with curvature correction for Reynolds-average Navier-Stokes (RANS) equation was used. Also, second-order upwind discretization in space was used. The convergence rate was monitored during the iteration process by means of the residuals of the dependent variables of the governing differential equations.

The external domain, which is a cylinder with height 6R and radius 3R (R is the blade length equal 3m), is shown in Fig.III.10. Domain entrance was defined as “Velocity Inlet” and exit was defined as “Pressure Outlet” boundary conditions. The outer domain's walls were defined as “Symmetry” boundary condition (Fig.III.11).

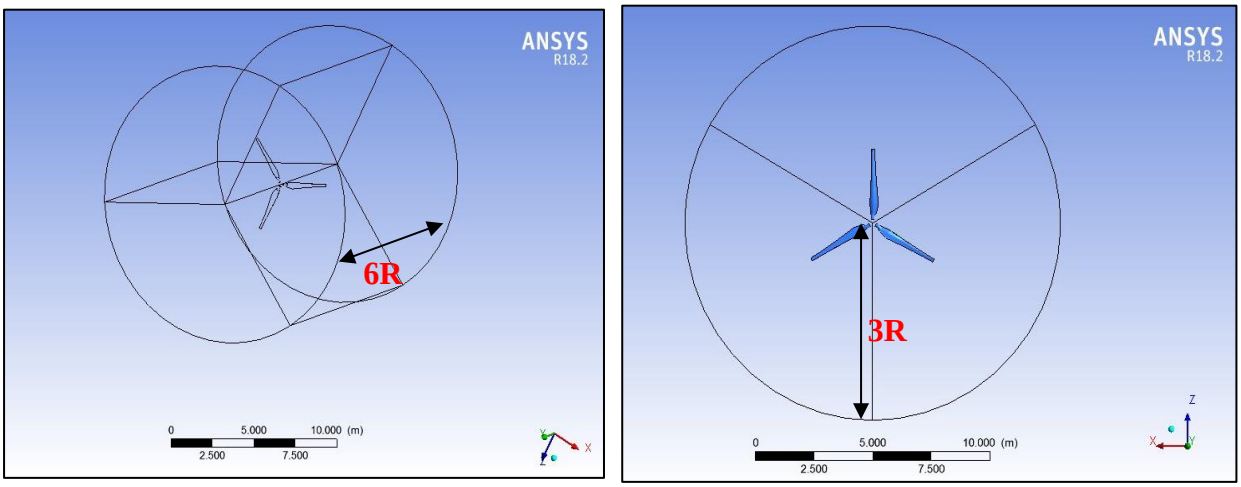

Figure III.6: The Flow domain with for 3D analysis

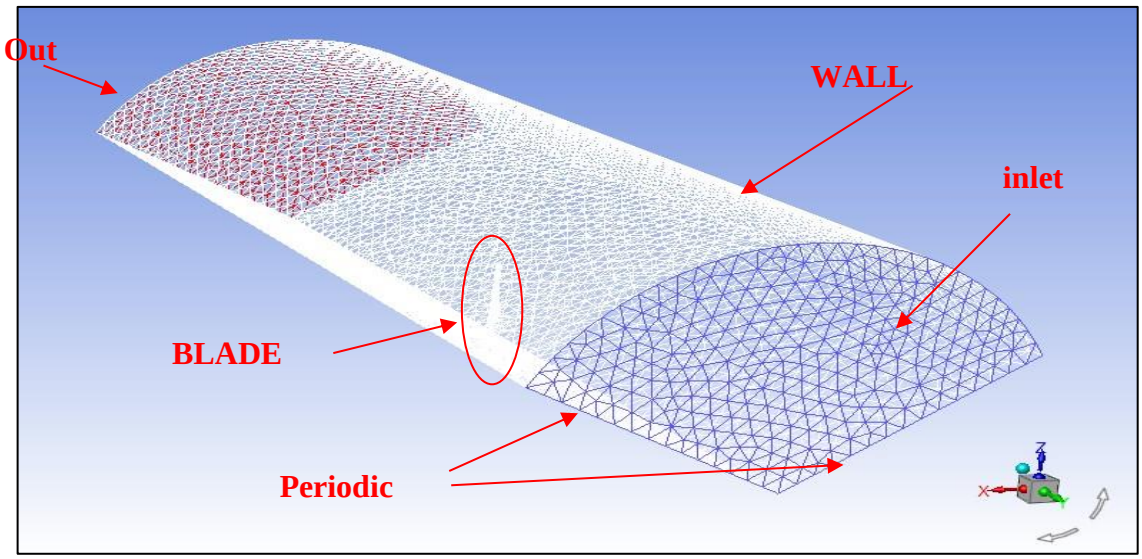

Figure III.7: Boundary conditions

The unstructured grid was applied on the turbine rotating disk area and external flow domain surrounding the turbine

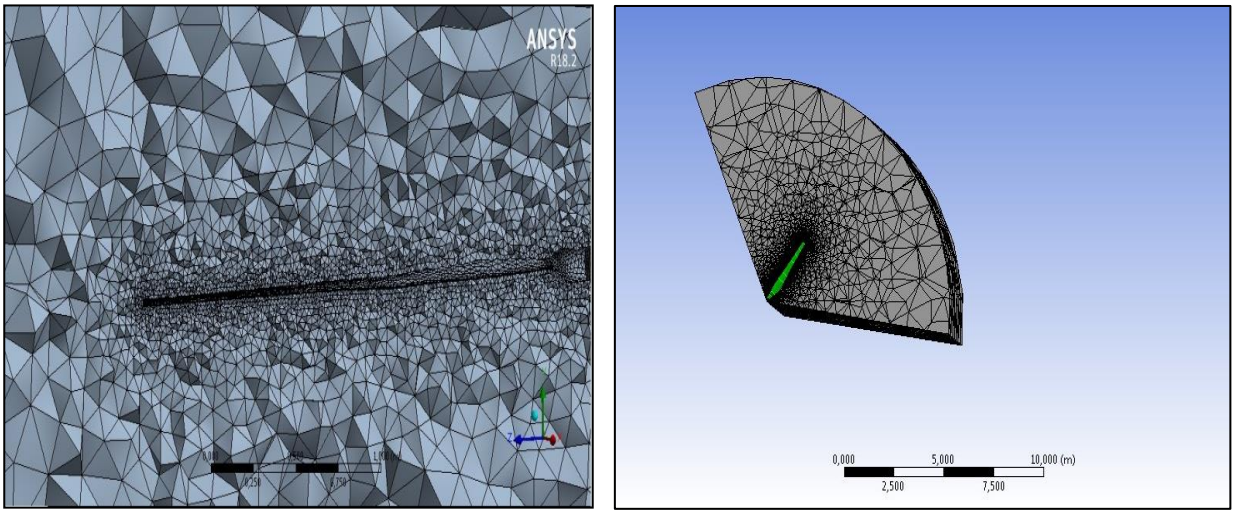

Figure III.8: The grid structure of the flow domain with the blade.

III.5.1. PRESSURE AND VELOCITY CONTOURS:

The analysis is done for various logical positions on the blade (0.26R, 0.47R, 0.68R and 0.9R). The pressure and the velocity contours are considered for analysis. The two contours at all the positions for a given wind speed are shown together (Fig.III.14, Fig.III.16, Fig.III.18, Fig.III.20, Fig.III.22, Fig.III.24, Fig.III.26 and Fig.III.28).

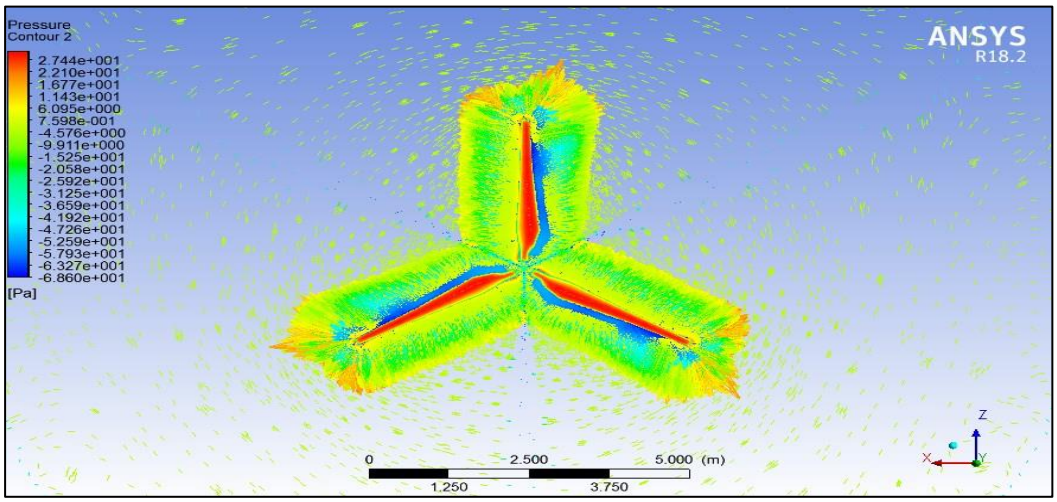

Figure III.9: Full wind turbine Pressure Contour with wind speed 7m/s.

Fig.III.14. Shows the distributions of the pressure field at r = 0.26R, r = 0.47R, r = 0.68R and r = 0.90R with V =7 m/s.

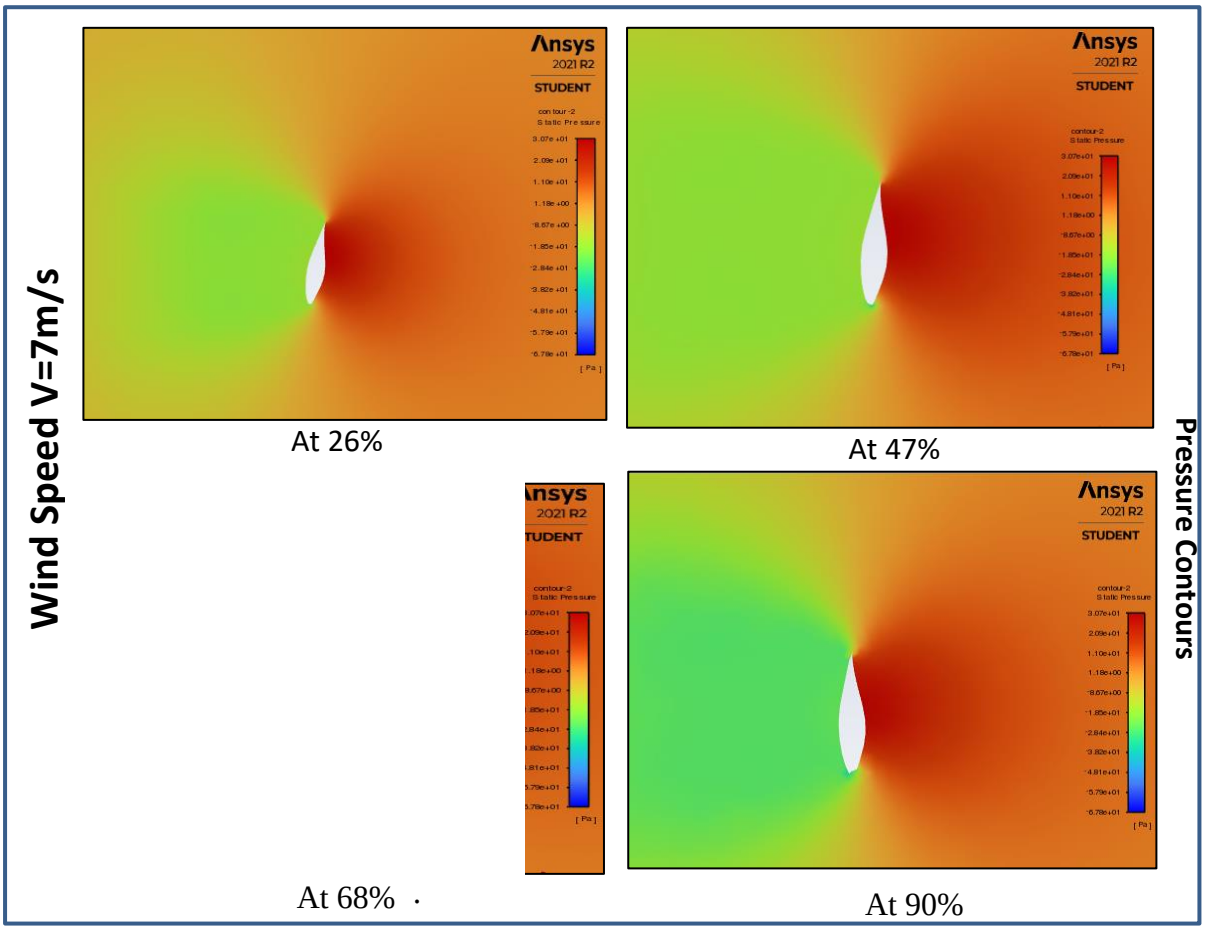

Figure III.10: Pressure contours with 7 m/s wind speed at different blade radial

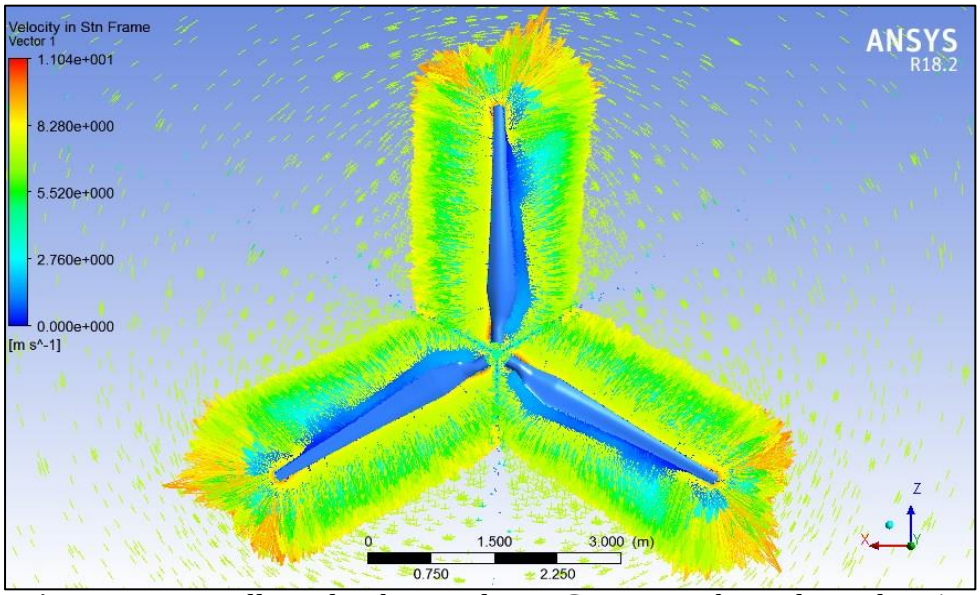

Figure III.11: Full wind turbine Velocity Contour with wind speed 7m/s.

Fig.III.16 Shows the distributions of the velocity field at r = 0.26R, r = 0.47R, r = 0.68R and r = 0.90R with V =7 m/s.

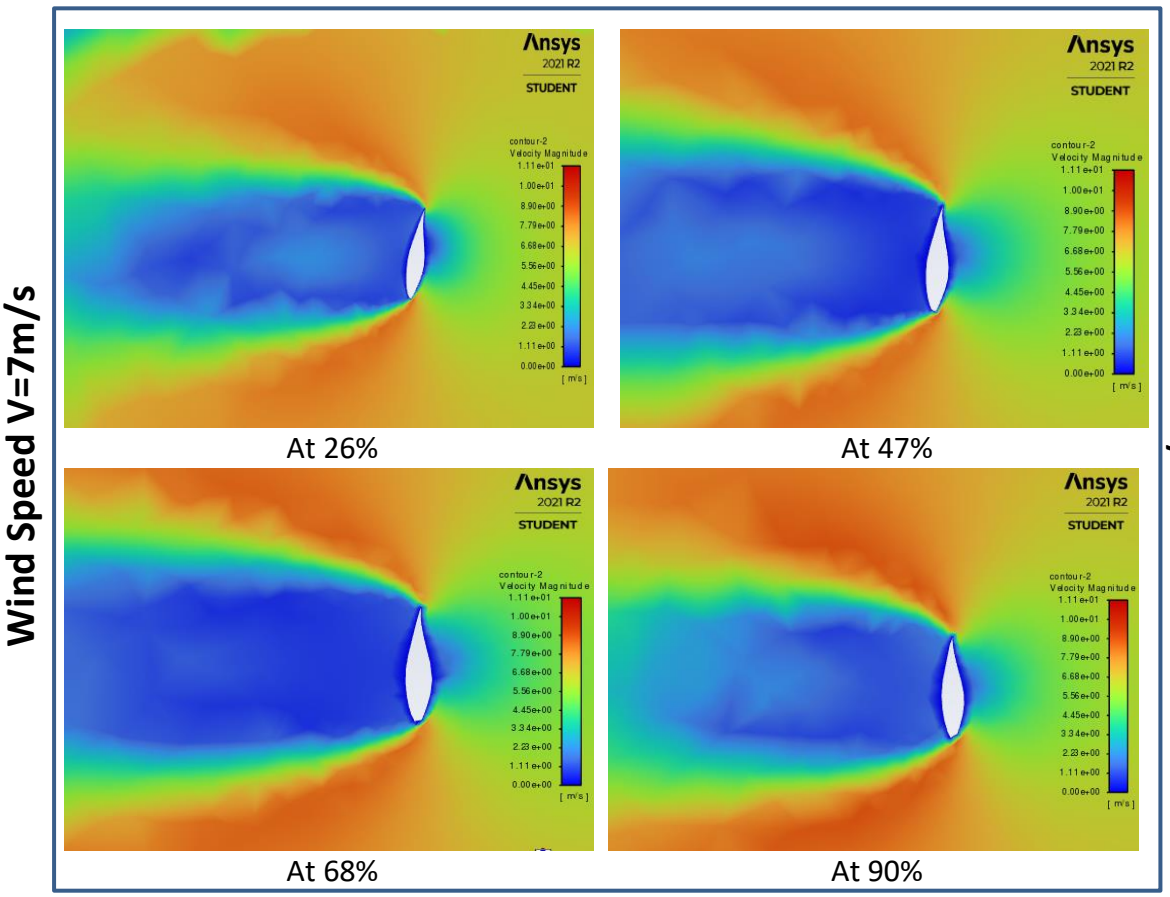

Figure III.12: Velocity contours with 7 m/s wind speed at different blade radial positions.

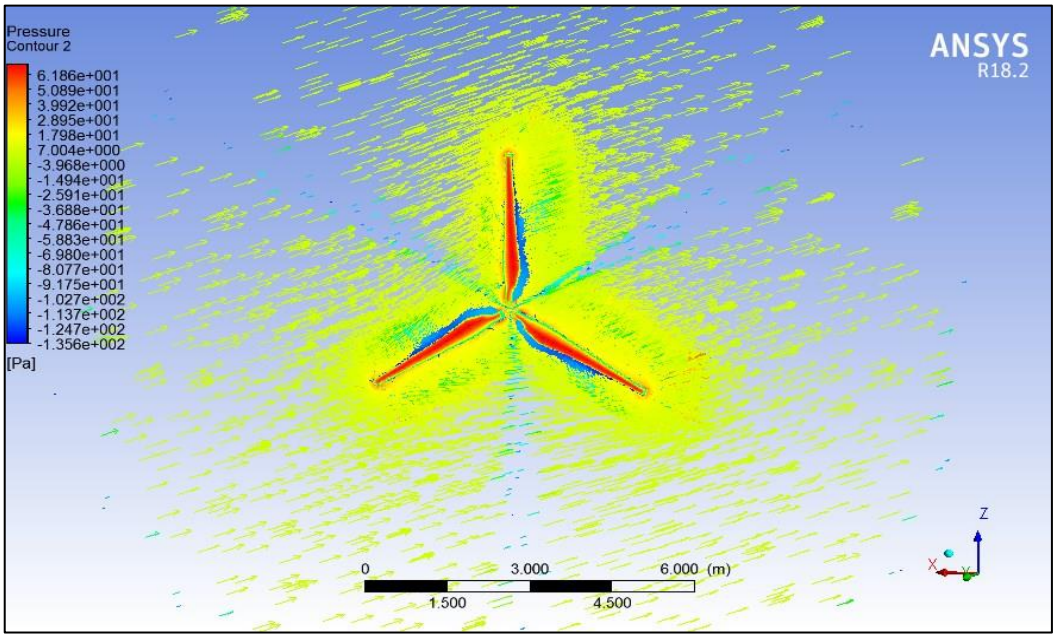

Figure III.13: Full wind turbine Pressure Contour with wind speed 10.5m/s.

Fig.III.18 Shows the distributions of the pressure field at r = 0.26R, r = 0.47R, r = 0.68R and r = 0.90R with V =10.5 m/s.

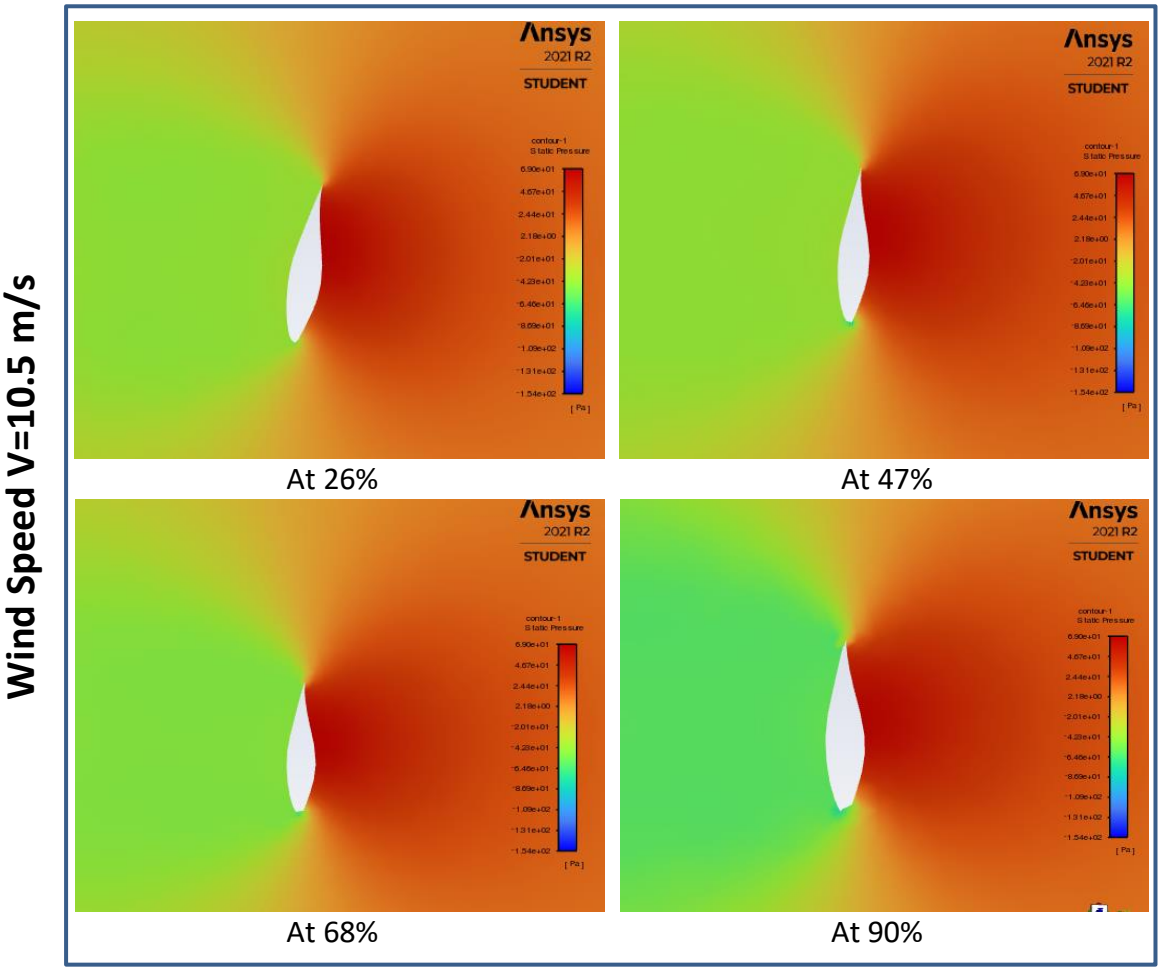

Figure III.14: Pressure contours with 10.5 m/s wind speed at different blade radial positions.

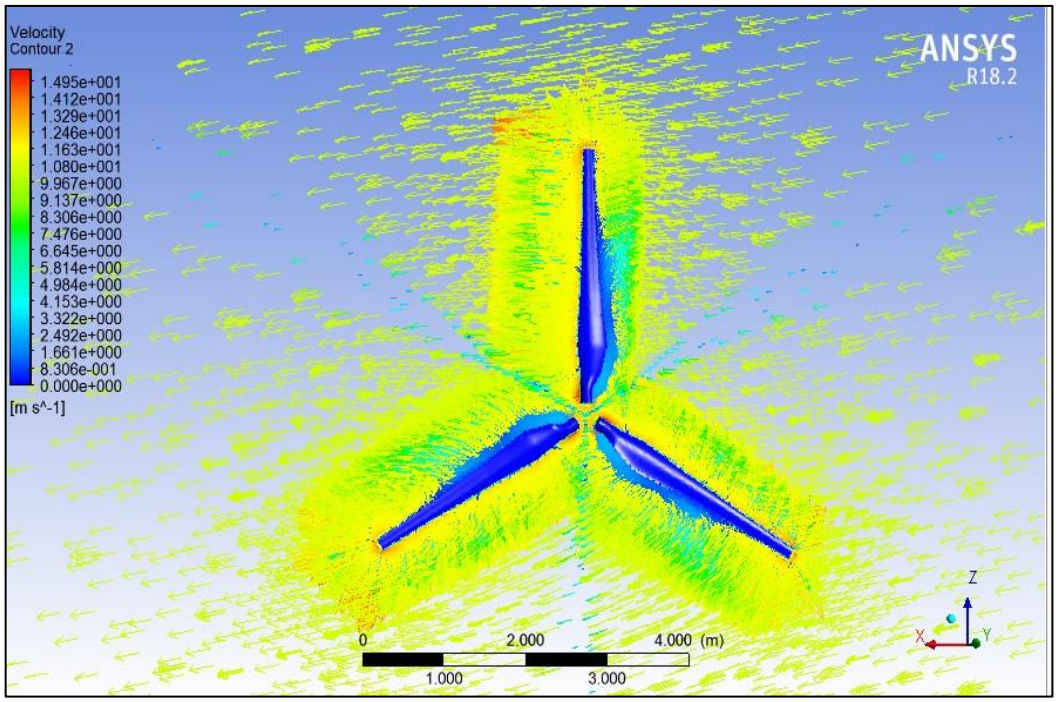

Figure III.15: Full wind turbine Velocity Contour with wind speed 10.5m/s.

Fig.III.20 Shows the distributions of the velocity field at r = 0.26R, r = 0.47R, r = 0.68R and r = 0.90R with V =10.5 m/s.

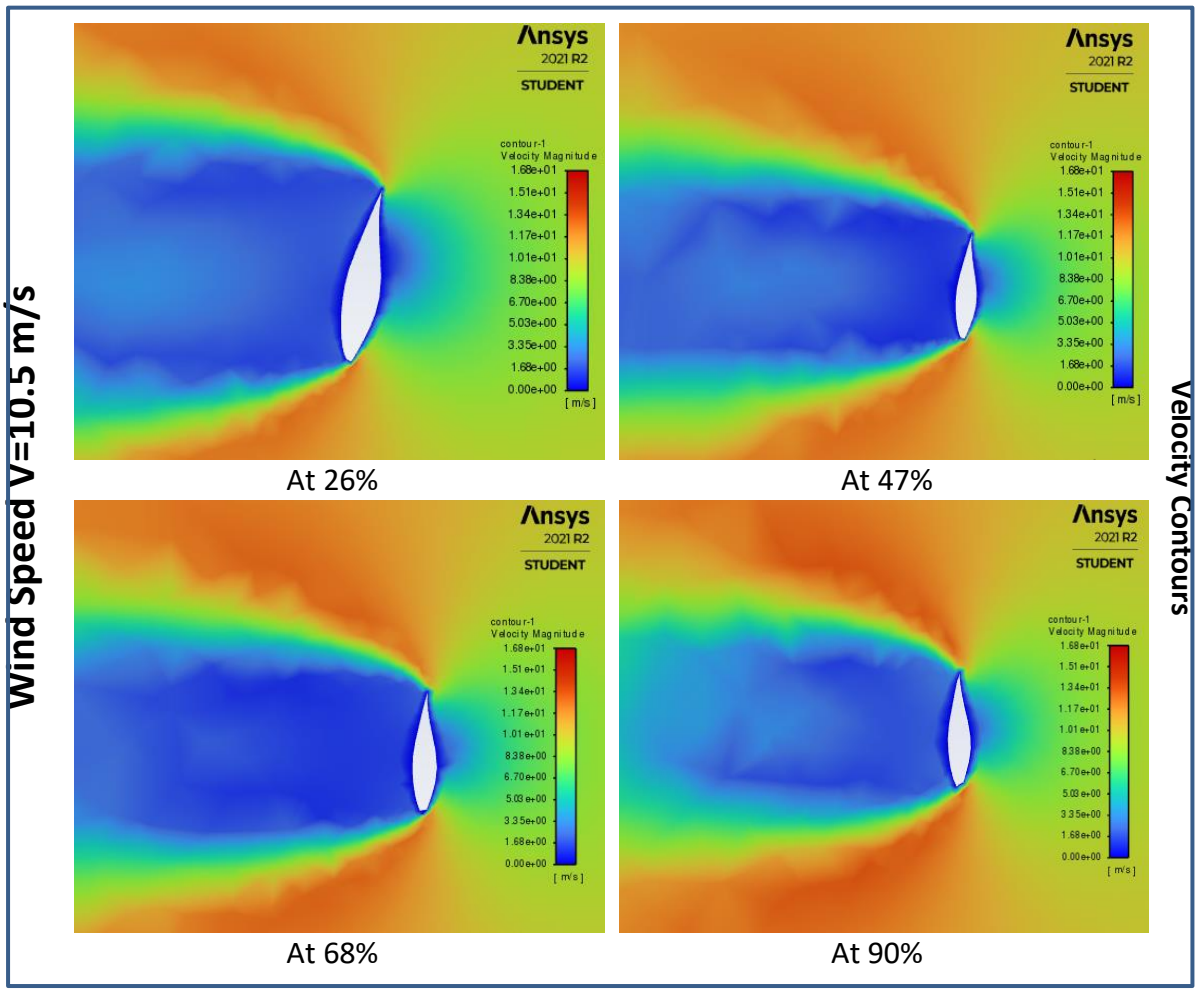

Figure III.16: Velocity contours with 10.5 m/s wind speed at different blade radial positions.

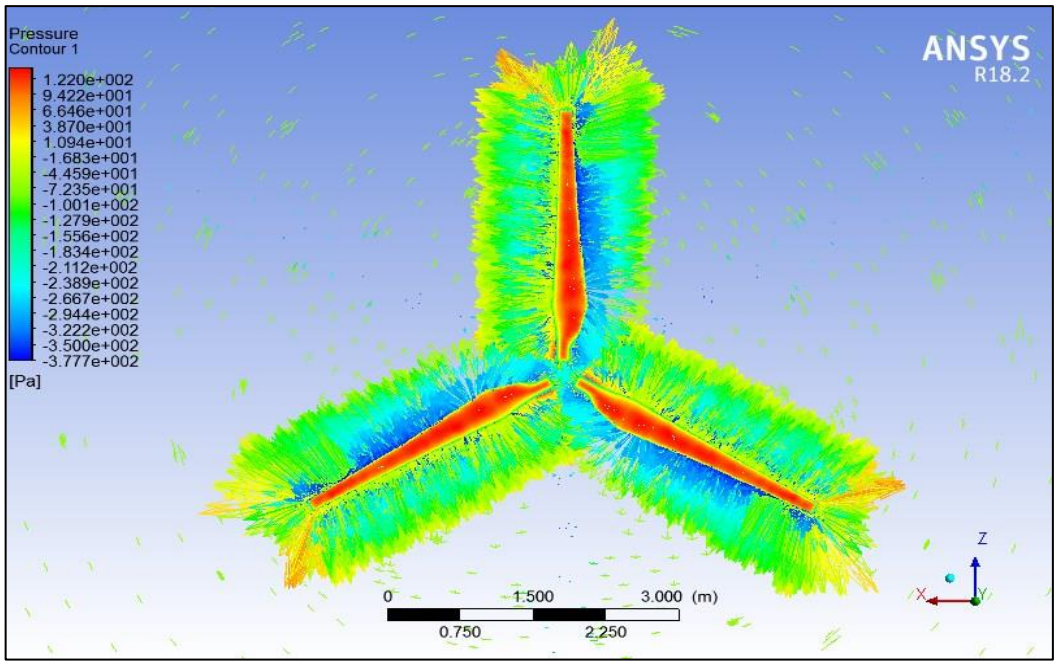

Figure III.17: Full wind turbine Pressure Contour with wind speed 15m/s.

Fig.III.22 Shows the distributions of the pressure field at r = 0.26R, r = 0.47R, r = 0.68R and r = 0.90R with V =15 m/s.

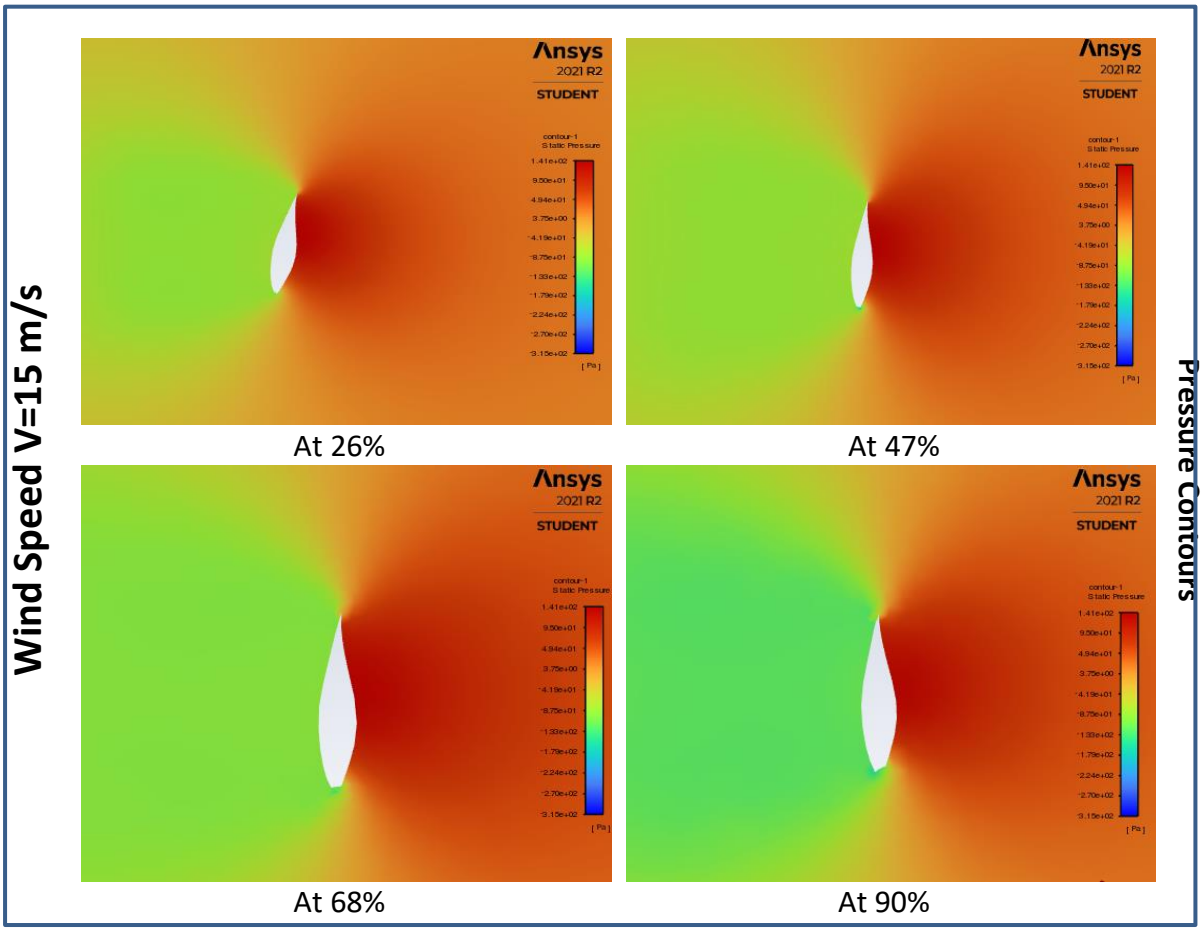

Figure III.18: Pressure contours with 15 m/s wind speed at different blade radial positions.

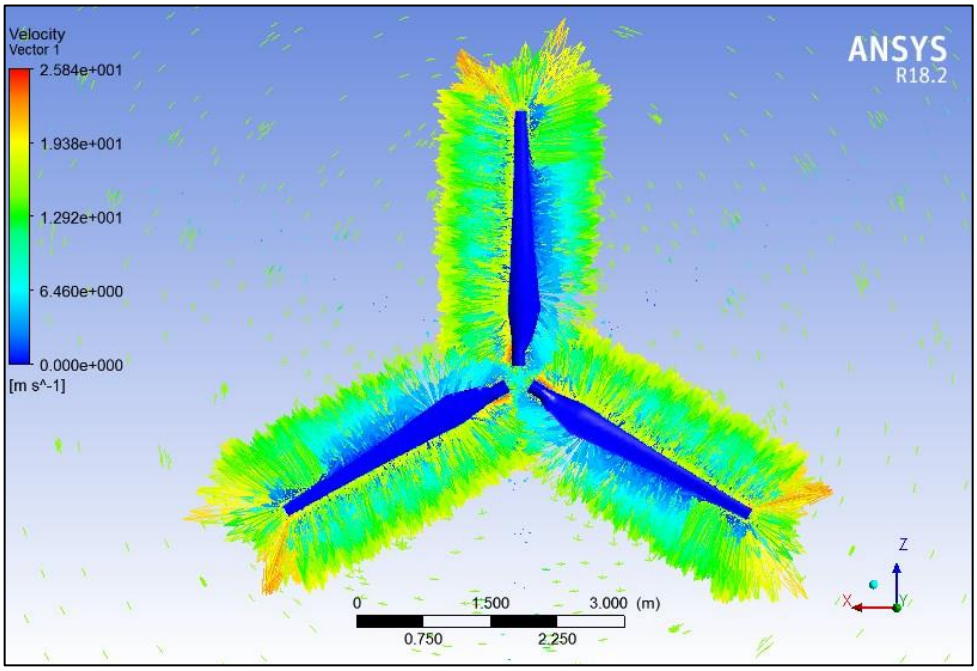

Figure III.19: Full wind turbine Velocity Contour with wind speed 15m/s.

Fig.III.24 Shows the distributions of the velocity field at r = 0.26R, r = 0.47R, r = 0.68R and r = 0.90R with V =15 m/s.

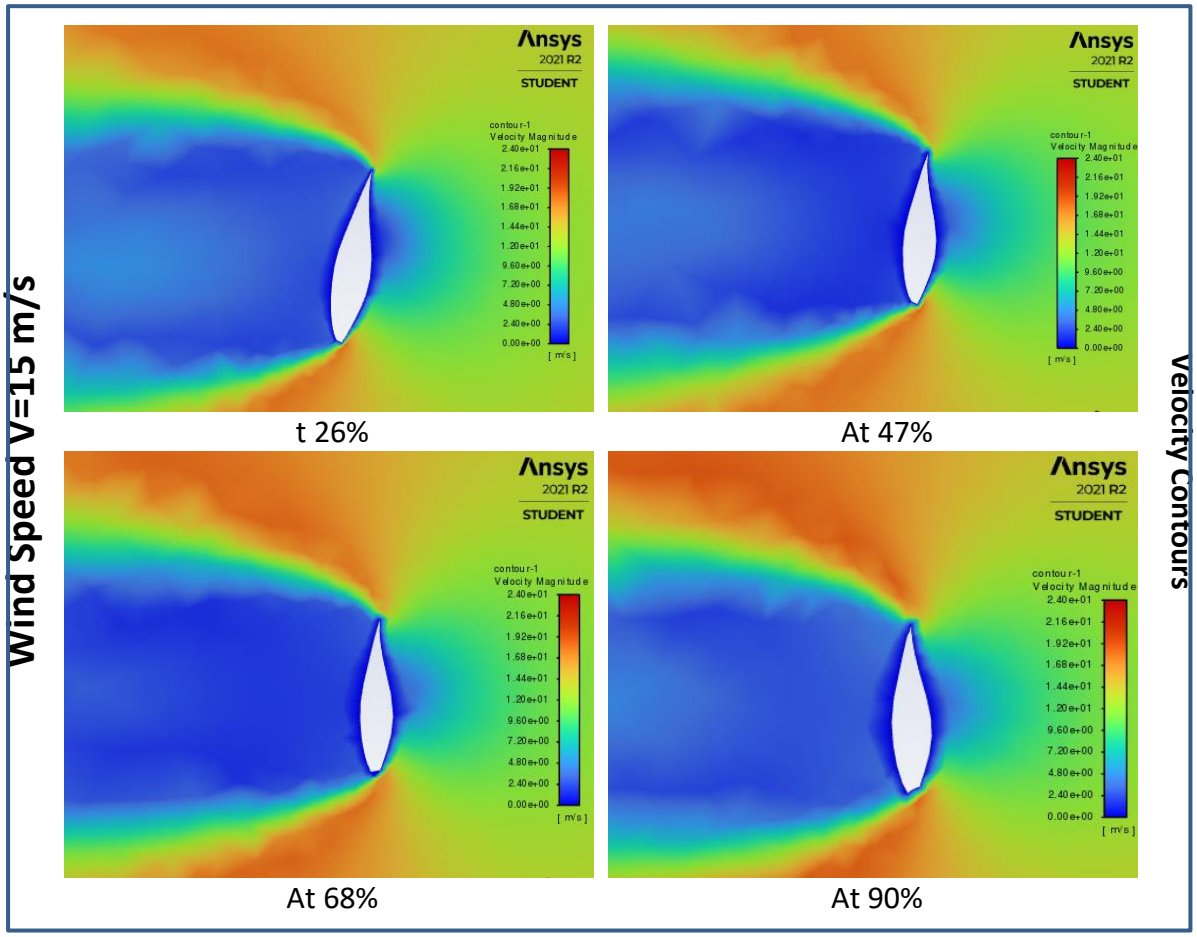

Figure III.20: Velocity contours with 15 m/s wind speed at different blade radial positions.

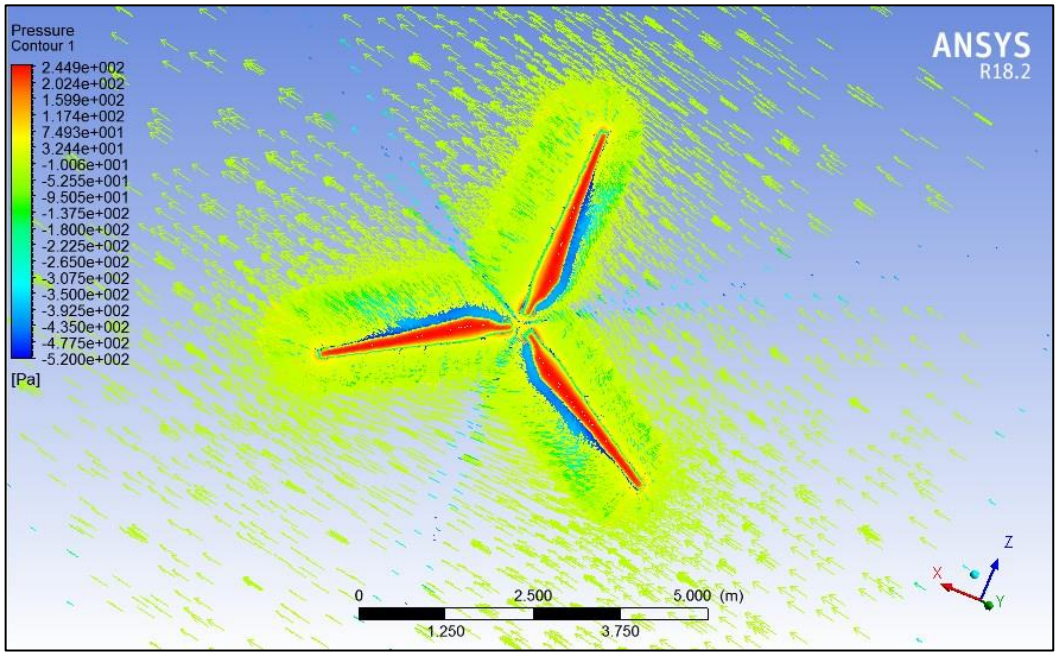

Figure III.21: Full wind turbine Pressure Contour with wind speed 20m/s.

Fig.III.26 Shows the distributions of the pressure field at r = 0.26R, r = 0.47R, r = 0.68R and r = 0.90R with V =20 m/s.

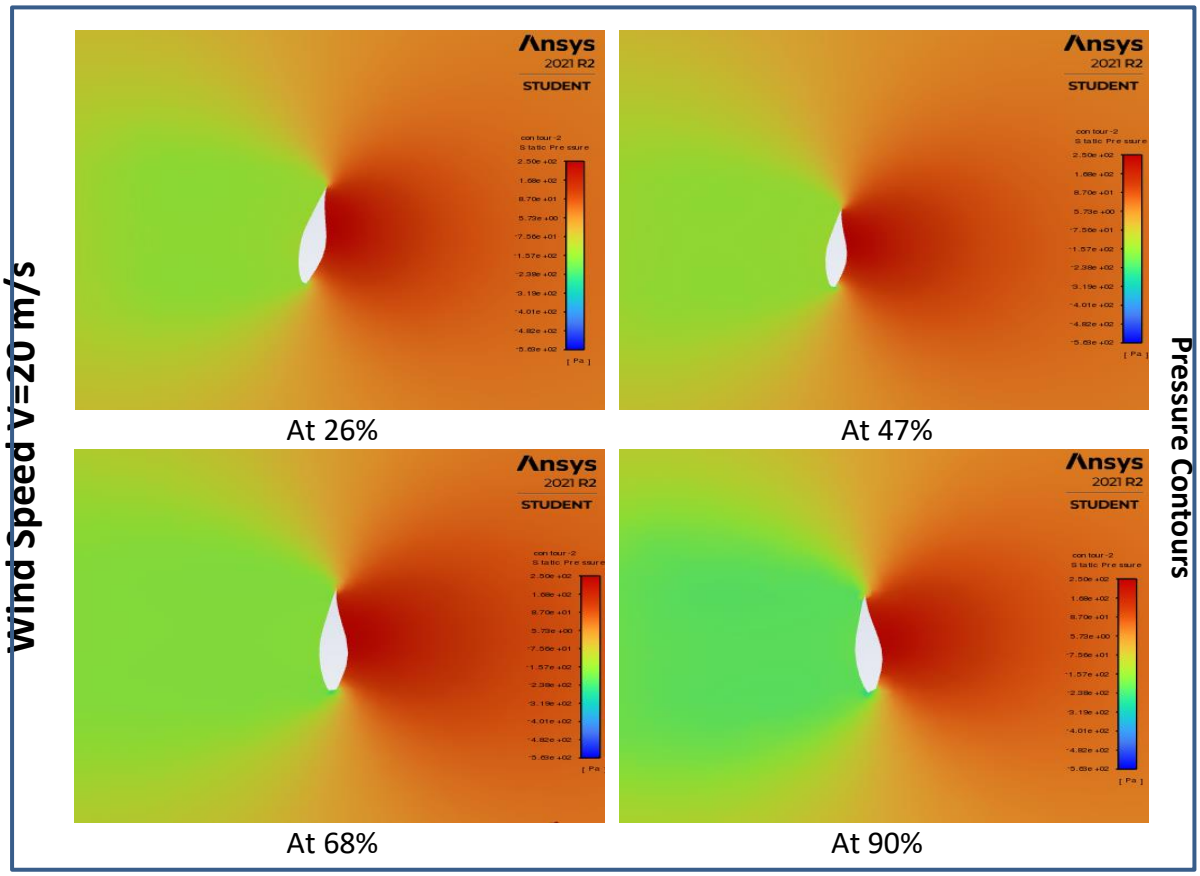

Figure III.22: Pressure contours with 20 m/s wind speed at different blade radial positions.

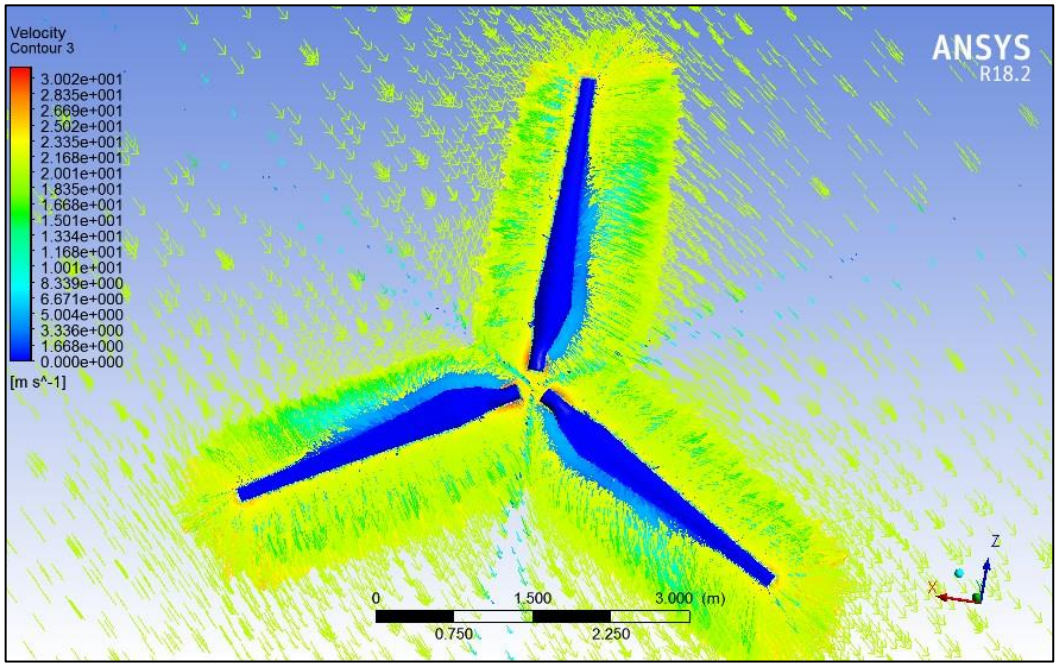

Figure III.23: Full wind turbine Velocity Contour with wind speed 20m/s.

Fig.III.28 Shows the distributions of the velocity field at r = 0.26R, r = 0.47R, r = 0.68R and r = 0.90R with V =20 m/s.

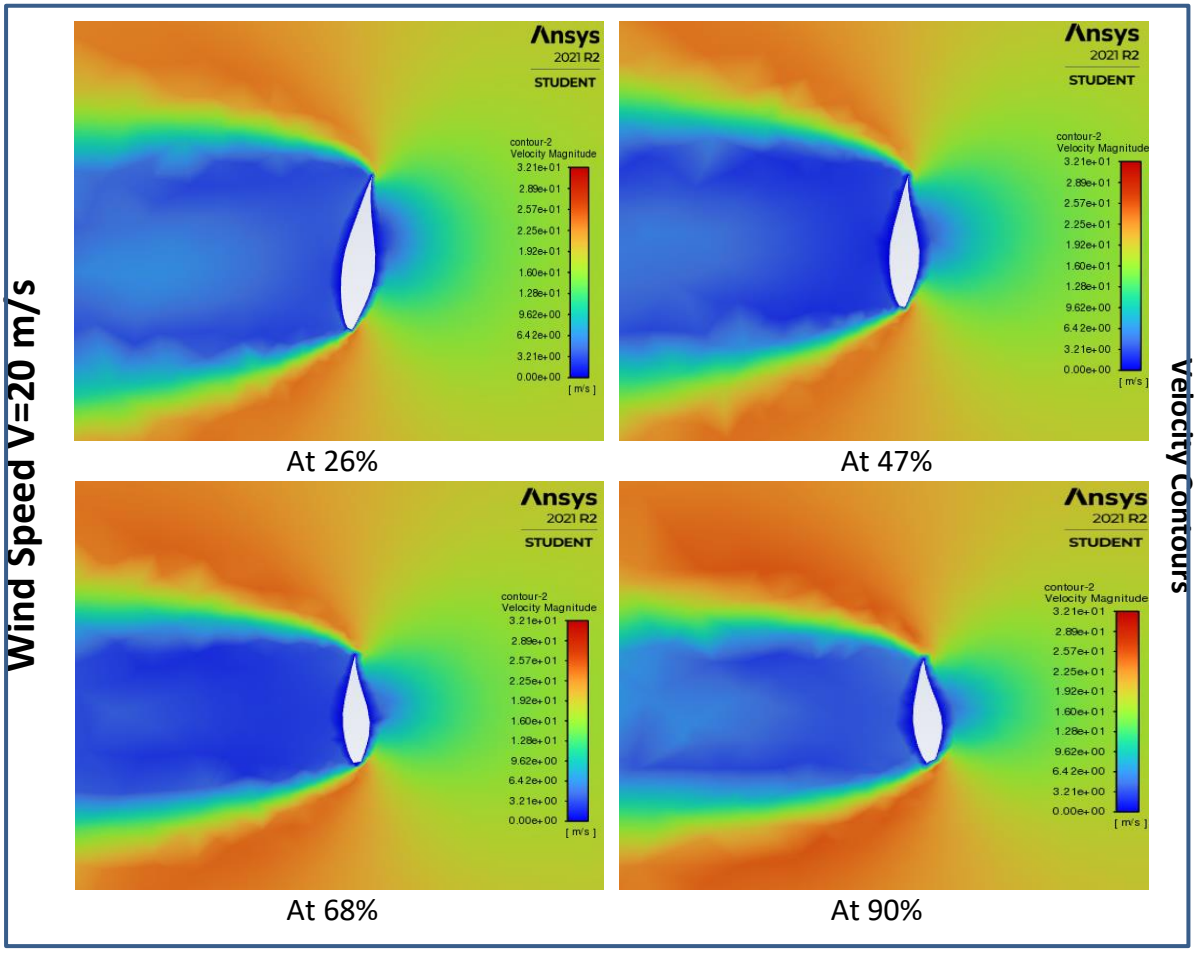

Figure III.24: Velocity contours with 20 m/s wind speed at different blade radial positions.

Based on 10 m/s of design wind speed, horizontal axis wind turbine performance analyses were performed by using Ansys-Fluent software. As results, the power and torque coefficients (Cp & Cm) values vs. various TSR graphics were obtained (Fig.III.25, Fig.III.26).

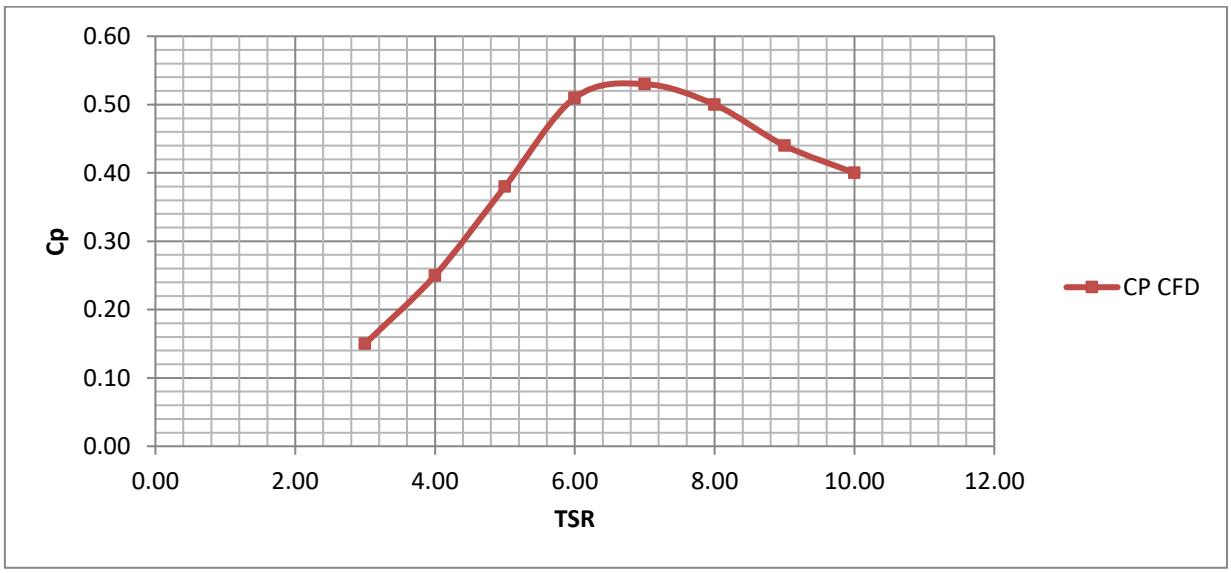

Figure III.25: The power coefficient versus tip speed ratio graphic using Ansys-Fluent software

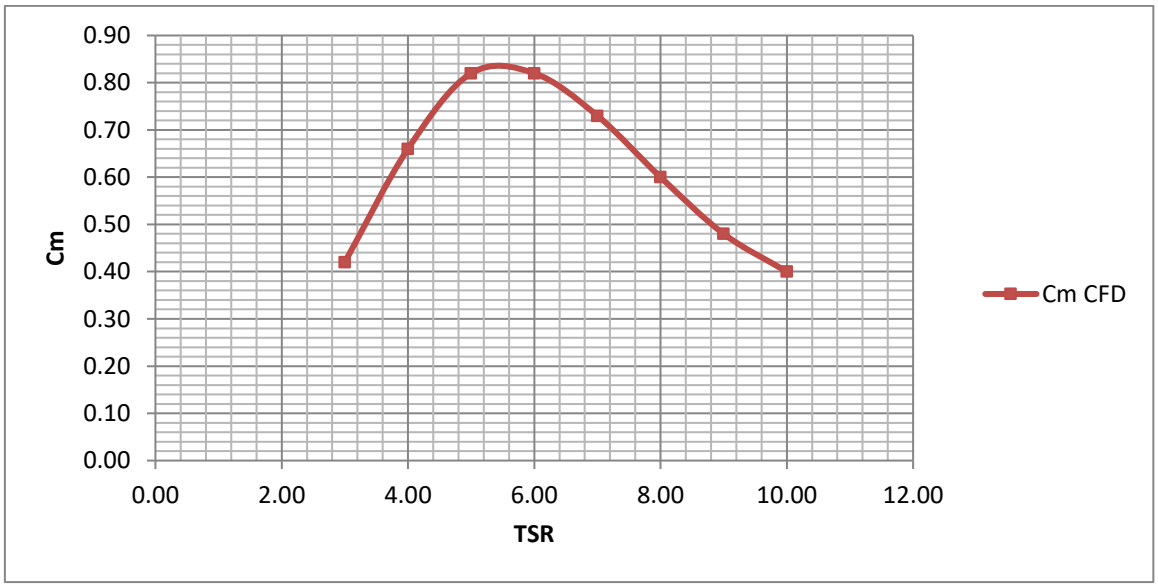

Figure III.26: The Torque coefficient versus tip speed ratio graphic using Ansys-Fluent software

III.5.2. COMPARATIVE STUDY BETWEED CFD & BEM RESULTS:

Figures Fig.III.27 & Fig.III.28 shows that initially at low TSR the performance & torque are very low and increased sharply in BEM, whether in CFD the Cp & Cm increased gradually with TSR up to 5. After that, in the BEM analysis, the Cp & Cm are more stable than in the CFD within the TSR range 5 to 7. For both cases, the maximum Cp has gotten at TSR 7 and the maximum Cm has gotten at TSR 6. After that, with the increasing of tip speed ratio, the coefficients of the performance and torque went down.

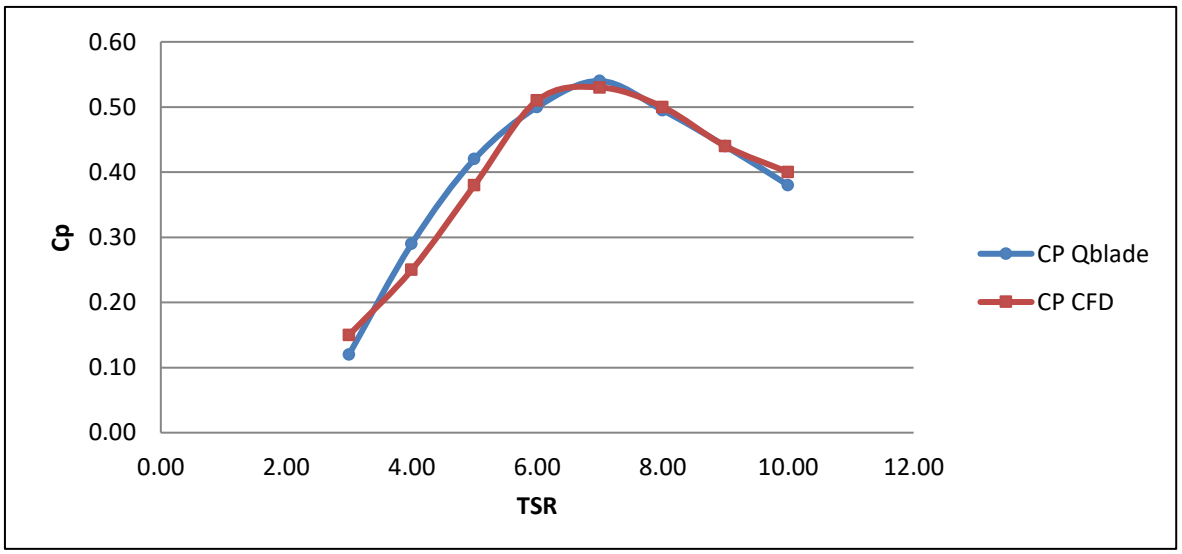

Figure III.27: Comparison of the power coefficients for wind turbine in Qblade and Fluent analyses.

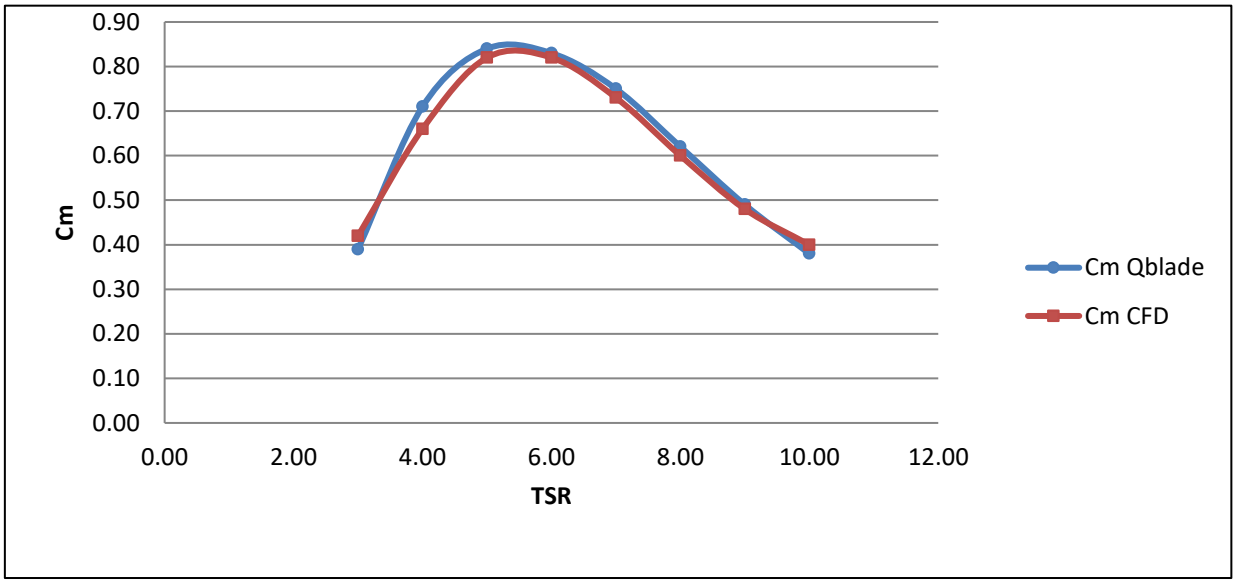

Figure III.28: Comparison of torques coefficient for wind turbine in Qblade and Fluent

III.6. Conclusion:

This study considered the performance characteristics of the wind turbine, which has an NREL S809 airfoil. Commercial code fluent with SST k-ω and the general public license QBlade, which uses BEM theory to predict aerodynamic coefficients, were used, respectively. The following conclusions were drawn:

Xflr5 software was used to obtain the values of the angle where the CL/CD ratio is maximum and the CLmax at this angle of attack. These values were obtained as 6.0 and 0.847, respectively..

The maximum torque coefficient value was achieved at a tip speed ratio of 0.84 in the Qblade and 0.82 in the Fluent. The maximum power coefficient value was achieved at 0.54 in Qblade and 0.53 in Fluent at tip speed ratio 7.

The efficiency of the system first increases and reaches the maximum value and then decreases with the increase of the tip speed ratio.

GENERAL CONCLUSION

GENERAL CONCLUSION:

The performance and torque coefficients of wind turbines were determined in this study using various tip speed ratios (TSRs). The wind turbine blade performance calculated using CFD is slightly lower than that calculated using BEM, as shown by the Cpvs TSR and Cm vs TSR curves. The reason for this is that the CFD approach can calculate 3D calculations more accurately than the BEM method.

Regardless of whether CP&CM in CFD progressively increases with TSR to 5, comparative graphs indicate that performance and torque are initially very poor at low TSR and rapidly increase in BEM. The TSR ranges between 5 and 7 in the BEM study, resulting in a more stable CFD than CP & Seymour. The maximum Cp has acquired at TSR7 and the maximum Cm obtained at TSR6 was noted in both cases. Following that, as the tip speed ratio increased, the coefficient of performance and torque decreased. The reason for this is the stall state of the wind turbine, which is specified by the wind turbine's Betz limit.

* In the BEM, the maximum coefficient of performance is 0.54, while in the CFD approach, it is 0.53. Both of these numbers are within the Betz range. The difference in outcomes between the two approaches is 1%.

* The highest coefficient of torque is 0.84 in BEM and 0.82 in CFD method.

*One reason for this difference is that, over prediction Xfoil software to obtain lift and drag coefficients.

* Despite the fact that the BEM included a variety of improvement models, the CFD findings provided more data on the wind turbine reaction, allowing for a more thorough understanding of the performance.

REFERENCES

REFERENCES

[1] J. Arramach, N. Boutammachte, A. Bouatem, A. Al Mers "Prediction of the Wind Turbine Performance by Using a Modified Assessing the feasibility of using the heat demand-outdoor" 2nd International Conference on Advances on Clean Energy Research, ICACER 2017,7-9 April 2017 Berlin, Germany

[2] Sandip. A. Kale, Ravindra N. Varma " Aerodynamic Design of a Horizontal Axis Micro Wind Turbine Blade Using NACA 4412 Profile" INTERNATIONAL JOURNAL of RENEWABLE ENERGY RESEARCH Sandip. A. Kale et al., Vol. 4, No. 1, 2014

[3] Sanjay Singh Bhadoria, Alok Kumar Maurya, Divya Singh, Vikas Kumar Wankar, Prashant Kumar, Vaishali Nehra Sharma " Materials for Wind Turbine Blades, Loading and Manufacturing Methods" International Journal of Engineering Research & Technology (IJERT) ISSN: 2278-0181 Published by, www.ijert.org ENCADEMS - 2020 Conference Proceedings

[4] Muhammad Fudhail, Sofian Mohd "Optimization of the Helical Wind Turbine Blade" Journal of Complex Flow, Vol. 3 No. 1 (2021) p. 1-6

[5] Vedulla Manoj Kumar, B Nageswara Rao, Sk. Farooq " Modeling and analysis of wind turbine blade with advanced materials by simulation "International Journal of Applied Engineering Research ISSN 0973-4562 Volume 11, Number 6 (2016) pp 4491-4499

[6] Er. Bharat Ankur Dogra, Dr. T. K. Jindal "Various Design Aspects of Wind Turbine Blades & a Measure to Analyze these Failures Due to Icing of Blades"IOSR Journal of Mechanical and Civil Engineering (IOSR-JMCE) e-ISSN: 2278-1684,p-ISSN: 2320-334X, Volume 12, Issue 2 Ver. IV (Mar - Apr. 2015), PP 06-12

[7] O.A.Abdul_Azim, S.M.Eldmerdash, K.M.Elshazly,O.E.Abdellatif " Experimental Investigation for Horizontal Wind Turbine of Direct-Drive" Benha Journal of Applied Sciences (BJAS) Vol.(2) Issue(1) Oct.(2017), 113-124

[8] L. Mishnaevsky Jr, K. Branner, H. Nørgaard Petersen, J.Beauson, M. McGugan and B. F. Sørensen "Materials for Wind Turbine Blades" materials 2017

[9] Peter J. Schubel, Richard J. Crossley"Wind Turbine Blade Design"Energies 2012

[10] C.M.Vivek, P.Gopikrishnan, R.Murugesh, R. Raja Mohamed " a review on vertical and horizontal axis wind turbine" International Research Journal of Engineering and Technology (IRJET) e-ISSN: 2395 -0056 p-ISSN: 2395-0072 Volume: 04 Issue: 04 Apr -2017

[11] S. K. Mutkule, P.P.Gorad, S.R.Raut, A.H.Nikam "Optimum and Reliable Material for Wind Turbine Blade" International Journal of Engineering Research & Technology (IJERT) ISSN: 2278-0181 Vol. 4 Issue 02, February-2015

[12] Sengul GUVEN "materials used in wind turbine blades and selection" International Journal of Scientific & Engineering Research Volume 9, Issue 7, July-2018 ISSN 2229-5518

[13] Bertagnolio, F.; Sørensen, Niels N.; Johansen, Jeppe; Fuglsang, P. "Wind turbine airfoil catalogue" Denmark.Forskningscenter Risoe. Risoe-R No. 1280(EN)

[14] Shafiqur Rehman, Md.Mahbub Alam, Luai M. Alhems and M. Mujahid Rafique "Horizontal AxisWind Turbine Blade Design Methodologies for Efficiency Enhancement—A Review" Energies 2018, 11, 506

[15] Martin O. L. Hansen, Aerodynamics of Wind Turbines, 3rd edition. Routledge. 2015

[16] Fei-Bin Hsiao, Chi-Jeng Bai and Wen-Tong Chong "The Performance Test of Three Different Horizontal Axis Wind Turbine (HAWT) Blade Shapes Using Experimental and Numerical Methods "Energies 2013, 6, 2784-2803.

[17] A. Hassanzadeh, A. H. Hassanabad, and A. Dadvand, "Aerodynamic shape optimization and analysis of small wind turbine blades employing the Viterna approach for post-stall region," Alexandria Engineering Journal, vol. 55, no. 3, pp. 2035-2043, 2016.

[18] K. M. Gierens, B. Kärcher, H. Mannstein, and B. Mayer, "Aerodynamically induced formation of contrails," in Proceedings of an International Conference on Transport, Atmosphere and Climate (TAC), 2007: Office for Official Publications of the European Communities, Luxembourg, pp. 267-272.

[19] R. Balijepalli, V. Chandramohan, and K. Kirankumar, "Optimized design and performance parameters for wind turbine blades of a solar updraft tower (SUT) plant using theories of Schmitz and aerodynamics forces," Sustainable Energy Technologies and Assessments, vol. 30, pp. 192-200, 2018.

[20] W. Su et al., "Research on Hydraulic Conversion Technology of Small Ocean Current Turbines for Low-Flow Current Energy Generation," Energies, vol. 14, no. 20, p. 6499, 2021.

REFERENCES OF FIGURE :

- **Figure I. 1** WIKIPEDIA
- **Figure I. 2** Magazine National Geographic, BYBRIAN CLARK HOWARD, PUBLISHED JANUARY 13, 2017 • 3 MIN READ
- **Figure I. 3** WIKIPEDIA

- **Figure I. 4** Jake Richardson
- **Figure I. 5** Stephan Matthiesen_Wind Turbine Compoments FUBRARY 17,2012 Wils)
- **Figure I. 6** Rybak, S.C.: Description of the 3 MW SWT-3 Wind Turbine. In: Bendix Corporation Energy, Environment and Technology Office, San Gorgonio Pass, California 2012
- **Figure I. 7** Desings of foundations for Wind Turbines, Henrik Svensson, Sweden 2010)
- **Figure I. 8** Longo, Riccardo; Nicastro, Patricia; Natalini, Matteo; Schito, Paolo; Mereu, Riccardo; Parente, Alessandro (August 2020).
- **Figure I. 9** Watson, James; Serrano, 11 November 2017. Retrieved 6 November 2016.
- **Figure I. 10** Qiuying Zhao, Jacob Ickes, Chunhua Sheng, Abdollah Afjeh, The University of Toledo May 20, 2014
- **Figure I. 11** Windpower Engineering & Development. 22 October 2019.
- **Figure I. 12** Darrieus turbine holded by guy-wire". Earthship Biotecture. Retrieved 18 September 2015.
- **Figure I. 13** Darrieus turbine shematic. Earthship Biotecture. Retrieved 18 September 2015.
- **Figure I. 14** The Wind Energy innovative systems CONFERENCE,COLORADO SPRINGS, COLORADO,MAY 23-25, 2021
- **Figure I. 15** Solari, Giovanni (2019). Wind Science and Engineering: Origins, Developments, Fundamentals and Advancements. Springer. p. 570.
- **Figure I. (16-17-18-19-20)** [12]
- **Figure II.1:** [18]
- **Figure II.2** Engineering ToolBox, (2013). Lift and Drag. [online] Available at: https://www.engineeringtoolbox.com/lift-drag-fluid-flow-d_1657**.**
- **Figure II.3** W.A. Timmer, C. Bak, in Advances in Wind Turbine Blade Design and Materials, 2013
- **Figure II.4 :** [19]
- **Figure II.5** P. Greaves, in Offshore Wind Farms, 2016
- **Figure II.6** Aerodynamic design and analysis of a 10 kW horizontal-axis wind
- turbine for Tainan, Taiwan,Received: 11 November 2015 / Accepted: 22 January 2016
- **Figure II.7** Ravi Ramamurti,William Sandberg Jun 2018
- **Figure II.8:** [20]